NASA TECHNICAL MEMORANDUM 102591
AVSCOM TECHNICAL MEMORANDUM 90-B-002

COMBINED EFFECT OF MATRIX CRACKING AND STRESS-FREE EDGE ON DELAMINATION

S. A. Salpekar and T. K. O'Brien

March 1990

National Aeronautics and
Space Administration

Langley Research Center
Hampton, Virginia 23665

US ARMY
AVIATION
SYSTEMS COMMAND
AVIATION R&T ACTIVITY

ABSTRACT

The effect of the stress-free edge on the growth of local delaminations initiating from a matrix crack in a composite laminate is investigated using a three dimensional finite element analysis. Two glass epoxy layups, $(0_2/90_4)_s$ and $(\pm 45/90_4)_s$, were modeled with a matrix crack in the central group of eight 90° plies, and delaminations initiating from the matrix cracks in the 0/90 and -45/90 interfaces, respectively. The analysis indicated that high tensile interlaminar normal stresses were present at the intersection (corner) of the matrix crack with the stress-free edge, suggesting that an opening (mode I) delamination may initiate at these intersections.

In order to analyse the strain energy release rates associated with delaminations that may form at the corners, three different configurations of the local delamination were assumed. One configuration was a uniform through-width strip growing normal to the matrix crack in the direction of the applied load. The other two configurations were triangular shaped delaminations, originating at the intersection of the matrix crack with the free edge, and growing away from the corner. The analysis of the uniform delamination indicated that the magnitude of both the total strain energy release rate, G_T, and its components increased near the free edges. This edge effect was symmetric for the $(0_2/90_4)_s$ layup. However, for the $(\pm 45/90_4)_s$ layup, the G distribution across the front was asymmetric, with

the total G and its components having higher values near one free edge than the other. For both layups, the G_I component was large at small delaminations lengths, but vanished once the delamination had reached a length of one ply thickness.

The second and third delamination configurations consisted of triangular shaped delaminations with straight fronts inclined at angles of 10.6° and 45°, respectively, to the matrix crack. The total G along the delamination front decreased sharply near the matrix crack for both configurations and increased sharply near the free edge for the 10.6° configuration. However, the total G distribution was fairly uniform in the middle of the delamination front for the 10.6° configuration. These inclined models suggest that if the exact geometry of the delamination front could be modeled, a uniform G distribution may be obtained across the entire front. However, because the contour of the delamination front is unknown initially, it may only be practical to model the uniform through-width delamination and use the peak values of G calculated near the free edges to predict delamination onset. For the layups modeled in this study, the total G values near the free edge agreed fairly well with a previously derived closed form solution. However, a convergence study may need to be conducted to have confidence that peak values of G calculated from three dimensional finite element analyses near the free edges are quantitatively correct.

INTRODUCTION

With the increased use of composite materials in primary aircraft structures, there is a need for understanding their failure mechanisms to better predict service life. Composite laminates subjected to monotonic tension and tension fatigue loading undergo a succession of various forms of damage before complete failure. These damage mechanisms include matrix ply cracking [1-3], edge delamination [4-6], and local delaminations arising from matrix ply cracks [7-10]. The progression of damage in a $(\pm 25/90_n)_s$ laminate is a good case study to examine the relationship between matrix cracks, edge delamination, and local delamination. This relationship was experimentally demonstrated in reference [10] for $(\pm 25/90_n)_s$ laminates where n varied from 1/2 to 8. The results are shown schematically in figure 1. Under monotonic tension loads, these laminates exhibited 90° matrix cracking for all values of $n \geq 1$ (fig. 1a). The laminates with $n \leq 3$ developed thumbnail shaped edge delaminations at the -25/90 interfaces, whereas the laminates with $n \geq 4$ developed local delaminations in the vicinity of 90° ply cracks (fig. 1b). The delaminated area of the local delaminations was greatest in the region where the matrix crack meets the free edge, indicating that the local delaminations form at these corners. These local delaminations give rise to strain concentrations through the laminate thickness and lead to laminate failure [7-9].

Several researchers have shown that the interlaminar fracture toughness of a composite material may be used to predict the delamination onset and growth [1,8,10,11]. The interlaminar fracture toughness values are expressed in terms of critical values of strain energy release rate. They may be obtained for pure mode I delamination using the double cantilever beam (DCB) test, and for pure mode II loading using the End-notched flexure (ENF) test, under monotonic or fatigue loading [12]. The strain energy release rate associated with a delamination under an applied loading is compared with an appropriate value of interlaminar fracture toughness to predict the onset and growth of the delamination. The purpose of this study was to evaluate the strain energy release rate associated with local delaminations, particularly in the proximity of the stress-free edge where largest delamination area was observed (fig. 1b), in order to extend this delamination methodology to more realistic cracked-laminate configurations.

Previously, Fish and Lee [13] performed a three-dimensional finite element analyses of $(0_2/90_n)_s$ glass epoxy laminates to study the effect of 90° matrix cracks growing from the free edge. The delamination was assumed to grow in from the corner at an angle of 45° to the matrix crack, and was approximated in the form of a saw tooth. The number of 90° plies was varied from 1 to 4, and the effect of changing the matrix crack length and the delamination length was analyzed. However, only the average strain energy release rate across the entire delamination front was evaluated. Their results did not agree well with a simplified closed form expression for the

total G associated with local delamination that was derived earlier by O'Brien [7]. Part of the motivation for this study was to resolve this discrepancy. To this end, the G_T distribution across the front was determined from the 3D finite element analysis, and the maximum value in the distribution was compared to the closed form equation.

In this study, the $(0_2/90_4)_s$ and $(\pm 45/90_4)_s$ glass epoxy laminates were analyzed using the finite element method. The effect of cracking in the 90° plies on the strain energy release rate for local delamination, particularly near the free edge, was evaluated. The G distribution across the delamination front, and the change in G with delamination growth, was obtained for three different orientations of the local delamination with the free edge. The virtual crack closure technique was used to calculate the strain energy release rates. The total G results were also compared with G_T values calculated using the closed form equation previously derived by O'Brien [7] for local delamination.

NOMENCLATURE

a	delamination length from a matrix crack measured along the x-axis
s	distance along an inclined delamination front
E_{11}, E_{22}, E_{33}	modulus of elasticity of a unidirectional lamina along and transverse to, the fiber direction
E_{lam}	axial laminate modulus before delamination
E_{ld}	modulus of a locally delaminated cross section
E^*	modulus of an edge delaminated laminate
G	strain energy release rate
G_T	total strain energy release rate
G_{av}	total strain energy release rate averaged along a delamination front
G_I, G_{II}, G_{III}	Mode I, Mode II, and Mode III components of strain energy release rate , respectively
G_{12}, G_{13}, G_{23}	shear moduli of a unidirectional lamina
h	ply thickness
m	number of delaminations growing from a matrix crack
n	number of plies
P	axial load

S	reciprocal of axial laminate modulus
t	laminate thickness
t_{ld}	thickness of a locally delaminated cross section
V_i	relative nodal displacements
F_i	nodal forces
w	laminate width
X, Y, Z	Cartesian coordinates
α	angle between matrix-crack and local delamination front
θ	fiber angle in degrees, measured counter-clockwise from x-axis
Δ	delamination increment
ϵ	axial laminate strain
ν_{12}, ν_{13}, ν_{23}	Poisson's ratio of a unidirectional lamina
σ_z	interlaminar normal stress
σ_o	remote axial stress

LAMINATE CONFIGURATION AND LOADING

When a $(\pm\theta/90_4)_s$ laminate is subjected to tension load, matrix cracks form in the eight 90 degree plies at several locations along the length of the laminate, as shown in figure 2. Subsequently, either edge delaminations will form between the $-\theta/90$ interface due to Poisson mismatch between the sublaminates (Ref.1 & Appendix), or local delaminations will form between the $-\theta/90$ interface due to the presence of the matrix crack [7]. In order to study the effect of these damage modes, a representative segment of the laminate containing a single matrix crack, as shown by the shaded area in figure 2 will be considered in the analysis.

Figure 3 shows the representative segment of the $(\pm\theta/90_4)_s$ glass epoxy laminate. The segment is 80h long, 50h wide, and 12h thick, where h is the ply thickness. The laminate segment was assumed to be long compared to the local delamination lengths modeled, which were 5h long. The laminate was chosen wide enough to capture the effects near the edges and in the interior. The matrix crack is located at the mid-point along the segment length. The origin of the cartesian coordinate system is selected at the point where the matrix crack meets the $-\theta/90$ interface at the free edge. Due to the symmetry of the laminate and loading about its mid-plane, only the upper half of the laminate was analyzed. The material properties used in the analysis, for the glass epoxy laminate, are given in Table 1. The in-plane

properties for a unidirectional ply (e.g.; E_{11}, E_{22}, G_{12}, ν_{12}) are same as those in reference 14. The out-of-plane properties (G_{13}, ν_{13}, G_{23}, ν_{23}) were assumed to be identical to the in-plane properties, and E_{33} was assumed equal to E_{22}. The laminate is subjected to a tension load by applying uniform outward displacements at its ends (x= -40h, 40h).

In this study, the three dimensional finite-element analyses of this laminate were performed to obtain the interlaminar stresses and the strain energy release rates associated with a local delamination starting from the matrix crack. Figure 3 shows the first configuration analyzed with a delamination growing uniformly in the x-direction from the 90^{o} matrix crack. Analyses for two other orientations of the local delaminations with the matrix crack were also performed (fig.4). The angle of the inclined delamination with the matrix crack was assumed to be $10.6^{o}$and 45^{o}, respectively. Quasi-three-dimensional (Q3D) analyses of the laminate were performed to obtain G values in the interior. A closed-form equation for G_T [7] was evaluated and compared with the 3-D finite element results.

3-D FINITE ELEMENT ANALYSIS

Finite Element Models:

Uniform Delamination Front:

The model consisted of 13935 nodes and 2808 twenty-node brick elements. The top view of the finite element mesh at the -θ/90 interface is shown in figure 5 and the discretization in the thickness direction is shown in figure 6. In figure 5, a fine mesh in the vicinity of the free edge (y=0) and near the matrix crack (x=0) is used to capture the presence of high stress gradients. For the same reasons, a fine mesh in the thickness direction near the -θ/90 interface shown in figure 6 is used. The smallest element size used, near the edge and also near the crack was one-eighth of a ply thickness. Multi-point constraints were provided at the -θ/90 interface, in the shaded area (on the z=0 plane) shown in figure 3. The multi-point constraints can be released independently in the x,y,z directions to model delamination growth. The symmetry conditions were applied on the z=-4h plane by imposing zero displacements in the vertical direction, and rigid body motions were constrained in the x and y directions.

Inclined Delamination Front:

Figure 4 shows the configuration of a delamination which is assumed to grow from the corner of the matrix crack and the free edge. The cartesian coordinate system of the previous analysis is retained. Figure 7 shows the top view of the finite element mesh at the delamination plane. The refinement used near the corner is shown in figure 8. The element size along the direction of delamination extension was 0.2 - 0.25 ply thicknesses in the xy plane, and the element size was 0.125h in the z (thickness)

direction. A total of 3906 twenty-node isoparametric elements, and 18944 nodes were used.

The analyses were performed for several delamination fronts, inclined at an angle of α=10.6^{o} with the crack. The delamination distance, a, was measured from the corner, in the x-direction. In order to study the effect on the strain energy release rate, of changing the angle, α, of the delamination front, another finite element model was generated which makes a 45 degree angle with the matrix crack (y-axis).

Evaluated Parameters:

Interlaminar Stresses:

The interlaminar normal stresses on the z=0 plane were obtained to identify the location for delamination initiation. The $(\pm 45/90_4)_s$ laminate, similar to that in figure 3, but containing only the matrix crack with no delamination, was analyzed. The variation of σ_z along laminate length and laminate width will be discussed.

Strain energy release Rates:

The strain energy release rate, G, was calculated using the Virtual Crack Closure Technique (VCCT) [15, 16] and explained below with reference to figure 9. The values V_1 through V_5 are the relative displacements between the corresponding top and bottom nodes behind the crack front, and F_1 through F_5 are the forces in the element ahead of the crack front, above the

delamination plane. The three modes of the strain energy release rate and the value of G_T are calculated using the following equations.

$$G_I = -\frac{1}{2w\Delta} \Sigma \left(V_i \times F_i \right)_{opening} \quad (1)$$

$$G_{II} = -\frac{1}{2w\Delta} \Sigma \left(V_i \times F_i \right)_{shearing} \quad (2)$$

$$G_{III} = -\frac{1}{2w\Delta} \Sigma \left(V_i \times F_i \right)_{tearing} \quad (3)$$

$$G_T = G_I + G_{II} + G_{III} \quad (4)$$

In the equations (1) - (4), Δ is the increment of delamination growth normal to the delamination front and w is the element width along the front. The values of Δ assumed in this analysis are in the range of 0.125h to 0.25h. The delamination length, a, was increased by releasing the multi-point constraints up to the delamination front. The multi-point constraint nodes in the assumed delamination area were completely released from each other in the first analysis. The nodes of the delaminated planes crossing into the opposite plane were constrained in the vertical (z) direction in the next analysis. The quantity G_{av} is calculated as an average of the G_T values along the entire delamination front.

In the uniform delamination analysis (fig. 5), the mesh is more refined near one free edge (y=0) than the other free edge (y=50h). Thus it is possible to use a fine mesh near the y=0 edge for a given size of the finite element model. Using this model, the results near both the edges can be obtained. For the $(0_2/90_4)_s$ laminate, the G values will be symmetric about the y=25h line and the results at the y=0 edge will be the same as the results at the y=50h. In the case of the $(\pm 45/90_4)_s$ laminate, two analyses need to be carried out to obtain the effects near the two edges. The analysis of the $(+45/-45/90_4)_s$ layup yields results at the y=0 edge. The second analysis was carried out for a $(-45/+45/90_4)_s$ layup. The results of this second analysis near y=0 edge are the same as those of the original $(\pm 45/90_4)_s$ layup at y=50h.

In the inclined delamination analyses, the VCCT was used to calculate the mode I and total strain energy release rate. Small inaccuracies may be present in the results of this analysis because the delamination front does not grow self-similarly. However, a fine mesh is used in the analysis to minimize the inaccuracies, and the results will give a valuable qualitative insight into the variation of G_I and total G along the delamination front.

QUASI-3D ANALYSIS

Quasi-three-dimensional (Q3D) finite element analysis [17] of a y=constant cross section of the laminate was also performed. The finite element discretization used in the Q3D analysis was the same as that used

for the 3-D model in the XZ plane in figure 6. The Q3D formulation assumes an infinitely wide laminate and analyzes a two dimensional cross-section with three degrees of freedom at each node. The results are representative of the laminate interior, (e.g. y=25h) away from the stress-free edges. The G_I and G_T values were calculated for three different values of delamination length, a, using the quasi-3D analysis.

CLOSED-FORM SOLUTION

The total G associated with local delaminations originating at matrix cracks may also be calculated from a previously derived closed-form equation [7] (see appendix) as

$$G = \frac{p^2}{2mw^2} \left(\frac{1}{t_{1d} E_{1d}} - \frac{1}{t E_{1am}} \right) \qquad (5)$$

where the terms in eq.(5) are defined in the Appendix.

RESULTS

Interlaminar Normal Stress:

Figure 10 shows a plot of the normalized interlaminar normal stress, σ_z/σ_o, along the laminate width at x=0.0625h and x=0.625h where σ_o is the remote axial stress on the laminate. The σ_z stresses are tensile. For

the plot at x/h= 0.0625, i.e., very near the crack, there is a sharp increase in the σ_z value near the free edge. The corresponding values of σ_z are much smaller for the x/h=0.625 plot, i.e., away from the influence of the matrix crack.

The variation of σ_z/σ_o along a line in the x-direction, one-half of a ply thickness inside the edge (y/h=0.5), is shown in figure 11. The σ_z increases sharply near the matrix crack.

Figures 10 - 11 indicate that steep gradients in the interlaminar normal stress exist near the corner of the matrix crack and the free edge on the z=0 plane. Therefore, this corner is a probable site for local delamination onset.

Results of the Uniform Delamination Analysis:

In the following section, the results of the Q3D analysis are first compared with interior solutions obtained from the full 3-D analysis. Next, the G_T and G_I distributions along the uniform delamination front will be presented for the $(0_2/90_4)_s$ and $(\pm 45/90_4)_s$ layups, also referred to as layups A and B, respectively. Finally, the variation of G_T with delamination length, a, from the 3-D analysis will be compared to the closed form solution [7]. The values of G_I, G_{II}, G_{III}, and G_T, will be normalized by ϵ^2/h in presenting the results, where ϵ is the remote axial strain and h

is the ply thickness. Distances, such as delamination length, will be normalized by the ply thickness, h.

Comparison of Q3D and 3-D Analyses:

The Q3D model analyzed represents a cross-section in the interior (y=25h) of the laminate. Figure 12 shows the variation of normalized G_I and G_T with change in normalized delamination length, for a/h< 1. There is a close agreement between the results of the Q3D analysis and the interior (10< y/h <40)) solutions of the 3-D analysis.

Normalized G-distributions along a uniform delamination front:

The distribution of normalized G_I, G_{II}, G_{III}, and G_T along the delamination front, for the $(0_2/ 90_4)_s$ laminate are shown in figure 13 for a delamination length of 4 ply thicknesses. The plots are assumed to be symmetric about y/h= 25, due to the symmetry of the laminate configuration and loading. The opening mode is zero along the front. The G_{II} component (shearing in the x-direction) is constant in the interior, to within about seven ply thicknesses of the free edge, and rises quickly near the edge. The mode III (shearing in the y-direction) is zero in the interior, and increases in magnitude as y/h approaches either one of the free edges. This plot shows that the strain energy release rates near the free edge are higher than in the interior of the laminate.

The distribution of normalized G_I, G_{II}, G_{III}, and G_T along the delamination front, for the $(0_2/\ 90_4)_s$ laminate are shown in figure 14 for a delamination length of 0.375 ply thicknesses. These results are similar to those at a/h=4.0; however, at this smaller delamination length a mode I component is also present. This mode I component is constant in the interior and increases near the free edge. The G_I value is small relative to the corresponding G_{II} value, but is higher than G_{III}.

The normalized G distributions for the $(\pm 45\ /90_4)_s$ layup at a/h=4.0 are shown in figure 15. The results are higher than the similar values in figure 13 for layup A. Furthermore, these distributions are asymmetric, with higher normalized G values near the y/h = 0 free edge than near the y/h=50 free edge.

Figure 16 shows normalized G-distributions for a/h= 0.375, and indicates the presence of mode I . The G_I rises more steeply near the y/h= 0 edge than near the y/h= 50 edge.

Mode I at small delamination length

The presence of the opening mode at small delamination length was observed in figures 14 & 16. The opening mode does not exist at higher delamination length (figures 13 & 15). Figure 17 shows that the normalized G_I decreases with increasing delamination length in Layup A, and vanishes before the delamination has grown as far as one ply thickness. The G_I is

higher close to the free edge (y/h= 0.375) compared to the interior (y/h= 25). A similar variation is observed for Layup B and is given in figure 18. The edge effect is more pronounced in Layup B than in A due to the presence of off-axis plies, which results in a higher Poisson mismatch (see Appendix).

Because G_I decreases with increasing local delamination length, delaminations that form from matrix cracks may initiate in mode I and then arrest shortly thereafter. This arrest has been observed for local delaminations that form when the laminate is subjected to monotonic loading [10].

Variation of G_T with Delamination length:

Figure 19 shows the plots of normalized G versus a/h at y=3h/8, 5h/8, and at y=25h (interior) for the $(0_2/90_4)_s$ layup. Normalized total G increases with increasing delamination length, but eventually approaches a constant asymptotic value for each plot. The G_T values closer to the edge are higher than those in the interior. The average normalized G is slightly higher than the interior value due to the influence of the free edge.The value of G_T from equation (5), normalized by ϵ^2/h where $\epsilon = P/wtE_{lam}$, is greater than the interior value, but is similar to G_T values calculated very close to the edge using the 3-D analysis (fig.19).

Figure 20 shows the plots of normalized G versus a/h at y=3h/8, 5h/8, and at y=25h (interior) for the $(\pm 45/90_4)_s$ layup. The above discussion of the variation of total G with delamination length for the $(0_2/90_4)_s$ layup is also valid in case of $(\pm 45/90_4)_s$ layup. However, the closed-form solution cannot sense the asymmetry in the G distribution for layup B (figures 15,16). Hence, it may be calculating the average of the peak G values near the two edges. In any event, a convergence study, using several mesh refinements, is needed to make quantitative comparisons of the closed form solution to the 3D finite element model.

Based on the occurrence of relatively high G_T and G_I values near the y/h= 0 edge in the uniform through-width delamination, the subsequent analyses will focus on the variation of strain energy release rate near that edge for the inclined delamination.

Delamination Contour near the free-edge

Experimental evidence shows that the local delamination has a curved contour near the corner where the matrix crack intersects the free edge (figure 1b, n≥4). This curved contour was approximated as a straight delamination front growing from the corner and inclined at an angle to the matrix crack. In order to obtain the approximate shape of the contour in the vicinity of the corner, the uniform delamination analysis was used. As discussed in an earlier section, the delamination faces are open across the entire width at small delamination lengths. When the delamination length,

a, was 0.875h as shown in figure 21, the delaminated faces crossed into one another in some part of the delamination area. Figure 21 also shows the curved line of demarcation between the crossed faces and the open faces. This line is obtained by joining the nodes bordering the crossover region by straight-line segments. The changing angles α of these line segments, measured counter-clockwise from the matrix crack, are shown in figure 21. The average of the two values of α close to the free edge (10.6°), was used in modeling the inclined delamination.

Results of the Inclined Delamination Analysis (α=10.6°):

The analysis was performed for both the layups analyzed in the earlier section, i.e. layup A, $(0_2 / 90_4)_s$, and layup B, $(\pm 45 / 90_4)_s$. Figure 22 shows the variation of normalized G_T along the delamination front for layup A, when a/h=4.5. The value x/h=0, which also corresponds to s/h=0, is the point where the front meets the matrix crack. The value of x/h=4.5 corresponds to the intersection of the front with the free edge. The G_T value increases steadily while approaching the free edge (x/h=4.5). The normalized G_T distribution for layup B in figure 23 increases gradually towards the edge in the central portion of the front, but rises steeply near the free-edge due to the high Poisson mismatch between the sublaminates (see Appendix). The G_I was zero for both of the layups at these large delamination lengths.

A second analysis was performed for a much smaller delamination length with a/h= 0.6. The variation of normalized G_I along the front for Layup B is shown in figure 24. The gradual increase in G_I, as x/h approaches zero, is due to the angle α being higher than that required to match the delamination profile near the corner (figure 21, y/h>3).

Figure 25 shows a similar variation of normalized G_I along the delamination front for Layup B, at a/h= 0.4. Comparing figures 24 and 25 shows that G_I has a higher value for a/h= 0.4 than for a/h=0.6. Hence, as was the case for the uniform delamination, G_I increases with decreasing a/h.

The change in the total G, averaged along the delamination front is plotted as a function of a/h in figure 26. The average total G approaches a constant value at large delamination lengths, for both layups. The G_T is lower for layup A than for layup B. The increase in total G at small delamination length in layup B is due to the increase in G_I, discussed in the previous section. A further analysis is needed to determine whether the total G at very small delamination lengths is higher than the constant value attained at larger delamination lengths.

Results of the Inclined Delamination Analysis (45^o):

The normalized G_T along a 45 degree front, shown in figure 27 for layup A, reaches a peak value at x/h near 1 and then decreases with increasing

values of x/h (or s/h). This is in contrast to the variation for a similar case at α= 10.6 degrees (figure 22), where normalized G_T gradually increases with increasing x/h. The normalized G_T along the front, for layup B, plotted in figure 28, illustrates the same trend as does Layup A. In contrast, the normalized G_T distribution for α=10.6^o shown in figure 23 was nearly uniform in the central region, but gradually increased with increasing x/h. Thus, for layup B, the assumed angle α= 10.6 yields a more uniform G_T distribution along the laminate front than α=45^o. The experimentally observed angle α may be higher near the free edge, and lower near the matrix crack, as observed for the delamination profile (figure 21). This suggests that the exact contour for the delamination front may need to be modelled to obtain a uniform G distribution.

As shown in figure 29, the variation of total G, averaged along the front, approaches a constant at higher a/h, for both layups.

CONCLUDING REMARKS

Composite laminates containing a matrix crack and subjected to axial tension were analyzed using the a three dimensional finite element analysis. Glass epoxy $(0_2/90_4)_s$ and $(\pm 45/90_4)_s$ layups were modeled. A matrix crack was assumed to be present in the group of eight 90° plies. Local delaminations,

were assumed to initiate from the matrix crack at the 0/90 and -45/90 interfaces, respectively. Three dimensional finite element analyses were carried out to evaluate the effect of the free edge on the growth of the local delaminations.

The interlaminar normal stress increased sharply in the vicinity of the corner where the matrix crack meets the free edge, thus indicating that this corner is a potential site for delamination onset. In order to analyze the strain energy release rates associated with delaminations that may form at the corners, three different configurations of the local delamination were assumed. One configuration was a uniform through-width strip growing normal to the matrix crack in the direction of the applied load. The other two configurations were triangular shaped delaminations, originating at the intersection of the matrix crack with the free edge, and growing away from the corner.

For both layups, the total G and its mode I component, calulated in the interior of the laminate width for the uniform through-width local delamination, matched G values obtained from a quasi-three dimensional finite element analysis. However, the strain energy release rate and its components, calculated from the three dimensional finite element model, had higher values near the free edge than in the interior for both layups. For the $(\pm 45/90_2)_s$ layup, the G distributions across the width of the delamination front were asymmetric, with higher G values at one corner than at the other.

For both layups, G_I was non-zero at small delamination lengths, but rapidly decreased with delamination growth, and vanished when the delamination reached a length of one ply thickness. The total G consisted primarily of G_{II} at delamination lengths greater than one ply thickness. For all delamination lengths, G_{III} was non-zero only near the free edges. The total G reached a constant value at delamination lengths of about four ply thicknesses in the interior as well as near the edges.

The second and third delamination configurations consisted of triangular shaped delaminations with straight fronts inclined at angles of 10.6° and 45^{o}, respectively, to the matrix crack. The total G across the delamination front deviated near the matrix crack and the free edge for both configurations. However, the total G distribution was fairly uniform in the middle of the delamination front for the 10.6° configuration. These inclined models suggest that if the exact geometry of the delamination front could be modeled, a uniform G distribution may be obtained across the entire front. However, because the contour of the delamination front is unknown initially, it may only be practical to model the uniform through-width delamination and use the peak values of G calculated near the free edges to predict delamination onset. For the through-width model of the layups in this study, total G values near the free edges agreed fairly well with a previously derived closed form solution. However, a convergence study may need to be conducted to have confidence that peak values of G calculated

from three dimensional finite element analyses near the free edges are quantitatively correct.

ACKNOWLEDGEMENT

This work was performed under NASA contract NAS1-18599.

The first author would like to thank Dr. K. N. Shivakumar for helpful discussions, and Dr. I.S. Raju for the use of his 3-D finite element computer program.

APPENDIX

Poisson mismatch and influence of delamination on stiffness

In reference [7], the effect of local delamination versus edge delamination on laminate stiffness was compared. The stiffness loss due to edge delamination was derived in reference [16] as

$$E^* = \sum_{i=1}^{m} \frac{E_i t_i}{t} \qquad \text{(A1)}$$

where m is the number of sublaminates formed by the delamination, E_i and t_i are the modulus (calculated from laminated plate theory) and thickness of the i^{th} sublaminate formed, and t is the original laminate thickness. The difference between E_{lam} and E^* will be greatest for laminates with the largest "Poisson mismatch". The term "Poisson mismatch" refers to the difference between the Poisson's ratio of the original laminate and the Poisson's ratios of the 90° plies and the sublaminates that are formed by the delamination. For example, table 2A shows the Poisson's ratio of the $(0_2/90_4)_s$ and $(\pm 45/90_4)_s$ layups, the 0_2 and (± 45) sublaminates formed by the delamination, and the 90° plies. The difference between the laminate Poisson's ratio and that of the sublaminates is greatest for the $(\pm 45/90_4)_s$

laminate. Hence, the $(\pm 45/90_4)_s$ layup has a larger Poisson mismatch than the $(0_2/90_4)_s$ layup.

This difference is also reflected in the difference between the laminated and delaminated moduli, E_{lam} and E^*, calculated from laminated plate theory. Table 2B lists the moduli for the laminates, sublaminates, and 90° plies, as well as E^* calculated from eq(A1). Also listed is the stiffness loss, E_{lam}-E^*, for the two layups. The $(0_2/90_4)_s$ layup has only a 0.6% loss in stiffness due to a delamination in the 0/90 interface, whereas the $(\pm 45/90_4)_s$ layup experiences a 7.2% loss in stiffness due to a delamination in the -45/90 interface. These stiffness losses reflect the loss in the constraint that the 90 degree plies originally had on the sublaminates when they were laminated. This stiffness loss is reflected in the strain energy release rate associated with edge delamination [16] given by

$$G = \frac{\epsilon^2 t}{2} (E_{lam} - E^*) \qquad (A2)$$

Because the $(0_2/90_4)_s$ layup has a lower value of $(E_{lam} - E^*)$ than the $(\pm 45/90_4)_s$ layup, it will have a lower strain energy release rate for the same applied strain, ϵ.

G_T due to Local delamination

Similar to the case of edge delamination, the local delaminations that form at the intersection of matrix cracks and the free edge will relax the constraint between the 90 degree plies and the sublaminates. However, these local delaminations will also reduce stiffness because of the lost load carrying capability of the cracked ply [7]. Hence, the stiffness loss, and corresponding strain energy release rate, associated with local delamination will be different than for edge delamination. An equation for the total G associated with local delaminations originating at matrix cracks was derived by O'Brien [7].

$$G = \frac{P^2}{2mw^2} \left(\frac{1}{t_{ld} E_{ld}} - \frac{1}{t E_{lam}} \right) \qquad (A3)$$

where P is the axial load, m is the number of delaminations growing from the matrix crack, and w is the laminate width. This equation assumes that the cracked 90 degree plies do not carry any load in the delaminated region. The thickness of the locally delaminated region carrying the load (i.e. the thickness of the uncracked plies) is denoted as t_{ld}, and has a modulus, E_{ld}, that is calculated from laminated plate theory. The thickness of the entire laminate is t, and the laminate modulus E_{lam} is also calculated using

laminated plate theory. Because the stiffness of the original laminate, E_{lam}, and the locally delaminated region, E_{ld}, are calculated using the 2-dimensional laminated plate theory, G in equation (A3) accounts for both the loss in constraint as well as the loss in load carrying capability of the cracked off-axis plies [7].

Using E^* from eq(A1) instead of E_{lam} in eq(A3) excludes the effect of Poisson mismatch and isolates the effect of losing the load carrying capability of the cracked plies. Hence, eq.(A3) becomes

$$G = \frac{P^2}{2mw^2} \left(\frac{1}{t_{ld} E_{ld}} - \frac{1}{t E^*} \right) \qquad (A4)$$

Total G values from equations (A3) and (A4), normalized by ϵ^2/h where $\epsilon = P/wtE_{lam}$, are listed in table 3. Comparing the results of equations A3 and A4 indicates that the contribution of Poisson mismatch to the strain energy release rate for local delamination is relatively small for Layup A, but is significantly greater for layup B.

REFERENCES

[1] Reifsnider, K.L., and Talug, A., "Analysis of Fatigue Damage in Composite Laminates," Int. J. of Fatigue, Vol.3, No.1, Jan. 1980, pp.3-11.

[2] Masters, J.E., and Reifsnider, K.L., "An Investigation of Cumulative Damage Development in Quasi-Isotropic Graphite/Epoxy Laminates," Damage in Composite Materials, ASTM STP 775, K. L. Reifsnider, Ed., American Society for Testing and Materials, 1982, pp. 40-62.

[3] Reifsnider, K. L., "Some Fundamental Aspects of the Fatigue and Fracture Response of Composite Materials," Proceedings of the 14th Annual Meeting of Society of Engineering Science, Lehigh University, Bethlehem, Pa. 14-16 Nov., 1977.

[4] O'Brien, T. K., "Mixed-Mode Strain Energy Release Rate Effects on Edge Delamination of Composites," Effects of Defects in Composite Materials, ASTM STP 836, American Society for Testing and Materials, 1984, pp. 125-142.

[5] Adams, D.F., Zimmerman, R.S., and Odom, E.,M., "Frequency and Load Ratio Effects on Critical Strain Energy Release Rate G_c Thresholds of Graphite/Epoxy Composites," Toughened Composites, ASTM STP 937, Norman J.Johnston, Ed., American Society for Testing and Materials, Philadelphia, 1987, pp. 242-259.

[6] Whitney, J.M., and Knight, M., "A Modified Free-Edge Delamination Speciman," Delamination and Debonding of Materials, ASTM STP 876, W.S.Johnson, Ed., American Society for Testing and Materials, Philadelphia, 1985, pp. 298-314.

[7] O'Brien, T.K., "Analysis of Local Delaminations and Their Influence on Composite Laminate Behavior," Delamination and Debonding of Materials, ASTM STP 876, W. S. Johnson, Ed., American Society for Testing and Materials, Philadelphia, 1985, pp. 282-297.

[8] O'Brien, T.K., Rigamonti, M., and Zanotti, C., "Tension Fatigue Analysis and Life Prediction for Composite Laminates," NASA TM 100549, October, 1988.

[9] O'Brien, T. K., "Towards a Damage Tolerence Philosophy for Composite Materials and Structures," Composite Materials: Testing and Design, ASTM STP 1059, American Society for Testing and Materials, Philadelphia, 1990.

[10] Crossman, F. W., and Wang, A. S. D., "The Dependence of Transverse Cracking and Delamination on Ply Thickness in Graphite/Epoxy Laminates," Damage in Composite Materials, ASTM STP 775, American Society for Testing and Materials, Philadelphia, 1982, pp.118-139.

[11] Murri, G. B., Salpekar, S. A., and O'Brien, T. K.,"Fatigue Delamination Onset in Tapered Composite Laminates," NASA TM 101673, 1989.

[12] Martin, R.H., and Murri, G.B., "Characterization of Mode I and Mode II Delamination growth and Thresholds in Graphite/PEEK composites,"

Composite Materials: Testing and Design, ASTM STP 1059, American Society for Testing and Materials, Philadelphia, 1990.

[13] Fish, J.C., and Lee, S.W.,"Three-Dimensional Analysis of Combined Free-Edge and Transverse-Crack-Tip Delamination," Composite Materials: Testing and Design, ASTM STP 1059, American Society for Testing and Materials, Philadelphia, 1990.

[14] Chan, W., S., Rogers, C., Aker, S., "Improvement of Edge Delamination Strength of Composite Laminates Using Adhesive Layers," Composite Materials:Testing and Design., ASTM STP 893, 1986, p.266.

[15] Shivakumar, K. N., Tan, P. W., and Newman, J. C., Jr., "A Virtual Crack Closure Technique for Calculating Stress-Intensity Factors for Cracked Three-Dimensional Bodies," Int. Jnl. Fract., Vol. 36, 1988, pp. R43-R50.

[16] Raju, I. S., Shivakumar, K. N., and Crews, J. C., Jr., "Three-Dimensional Elastic Analysis of a Composite Double Cantilever Beam Specimen" AIAA Journal, Vol. 26, Number 12, December 1988, Pages 1493-1498.

[17] Raju, I.S., Q3DG- A Computer program for strain energy release rates for delamination growth in composite laminates, NASA CR-178205 (November 1986)

TABLE 1: MATERIAL PROPERTIES USED IN THE ANALYSES

S2/SP250 GLASS/EPOXY:

E_{11} = 7.30 MSI

E_{22}, E_{33} = 2.10 MSI

G_{12}, G_{13}, G_{23} = 0.88 MSI

ν_{12}, ν_{13}, ν_{23} = 0.275

TABLE 2 - STIFFNESS AND POISSON'S RATIOS OF LAMINATES AND SUBLAMINATES

A. POISSON'S RATIO, (in./in.)

Layup	ν_{lam}	ν_{90}	ν_{sub}	$\nu_{sub} - \nu_{lam}$	$\nu_{lam} - \nu_{90}$
$(0_2/90_4)_s$	0.104	0.079	0.275	0.171	0.025
$(\pm 45/90_4)_s$	0.162	0.079	0.508	0.346	0.083

B. STIFFNESS, ($x10^6$ psi)

Layup	E_{lam}	E_{90}	E_{sub}	E^*	$E_{lam} - E^*$
$(0_2/90_4)_s$	3.857	2.100	7.300	3.833	0.024
$(\pm 45/90_4)_s$	2.462	2.100	2.654	2.285	0.177

TABLE 3 - NORMALIZED STRAIN ENERGY RELEASE RATE VALUES FOR LOCAL DELAMINATION

Layup	Gh/ϵ^2 (eq.A3) $\times 10^6$	Gh/ϵ^2 (eq.A4) $\times 10^6$	(eq.A3 - eq.A4) $\times 10^6$
$(0_2/90_4)_s$	6.77	6.61	0.16
$(\pm 45/90_4)_s$	13.16	10.84	2.32

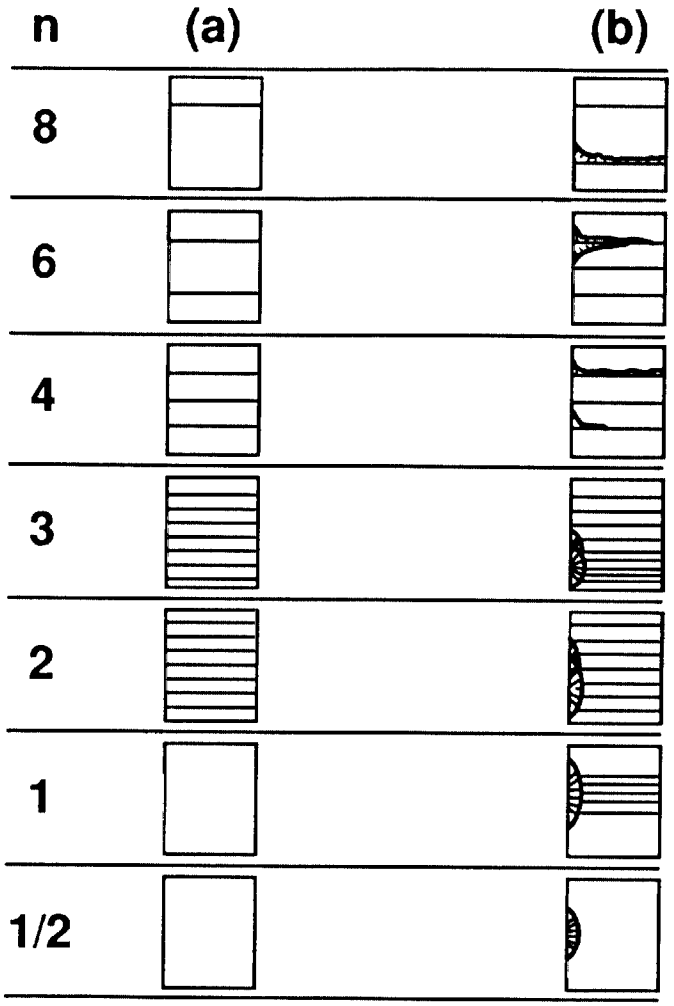

Fig. 1- Schematic of the fracture sequence in the $(\pm 25/90_n)_s$ laminates: (a) just prior to edge delamination, (b) subsequent to edge delamination [Ref.10].

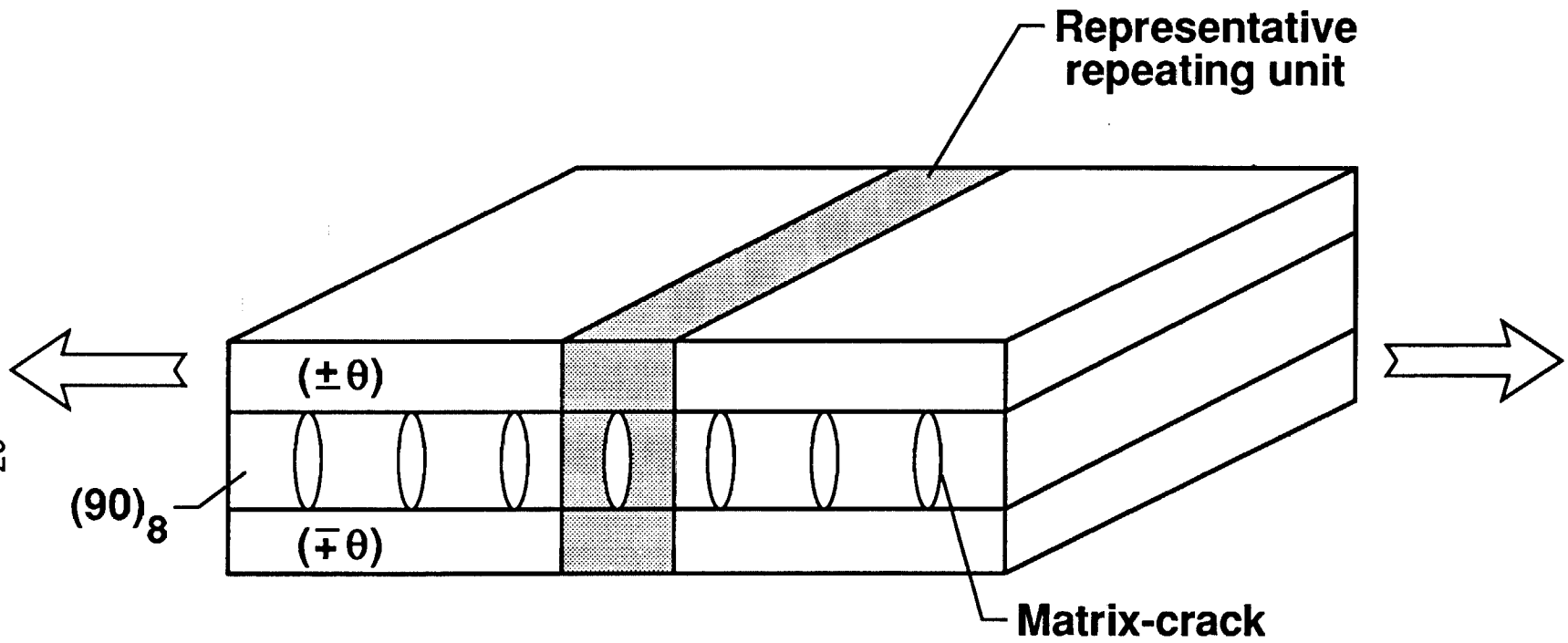

Fig. 2- $[\pm\theta\ /90_4]_s$ laminate with matrix cracks.

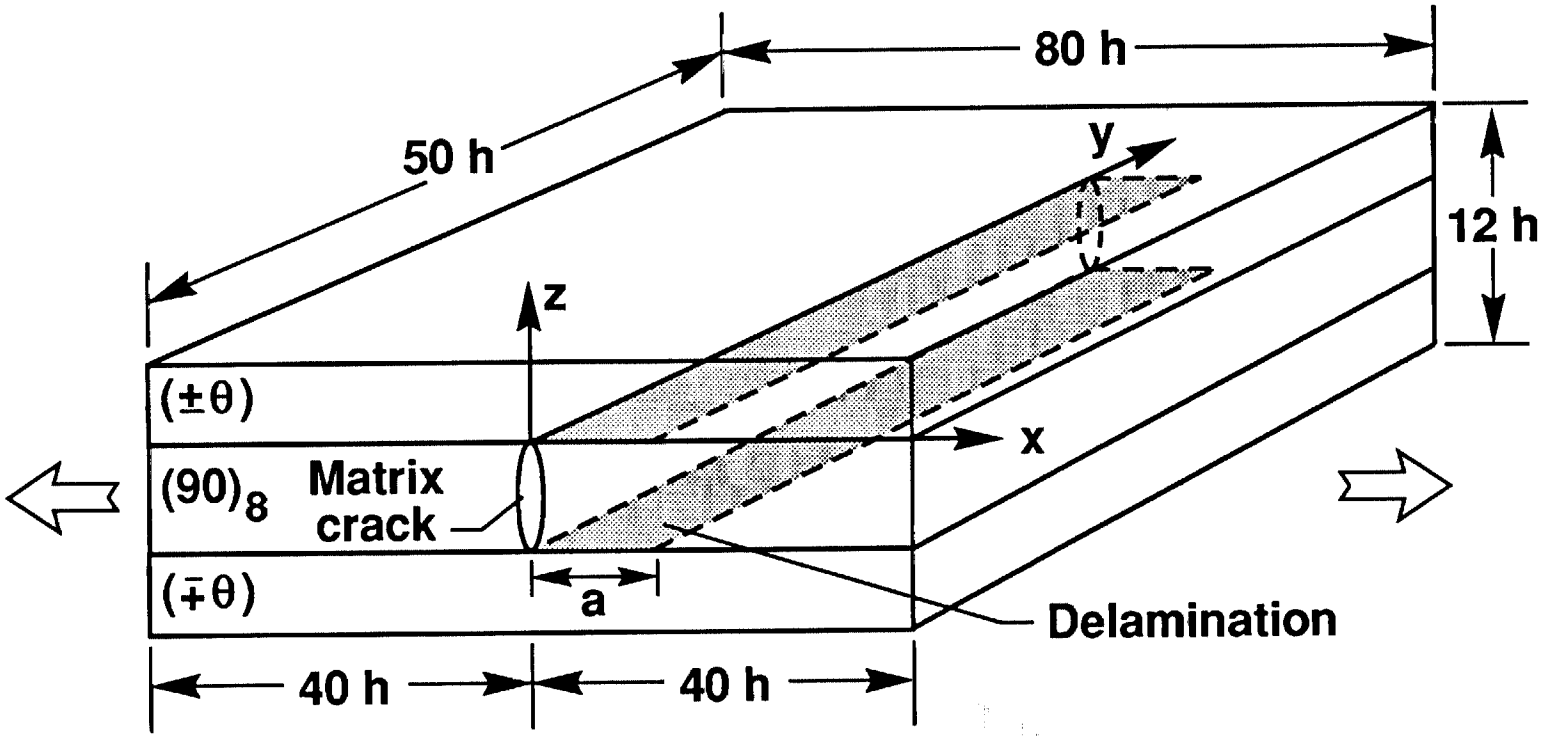

Fig. 3- Schematic of a uniform through-width delamination, growing from a 90^{o} matrix crack.

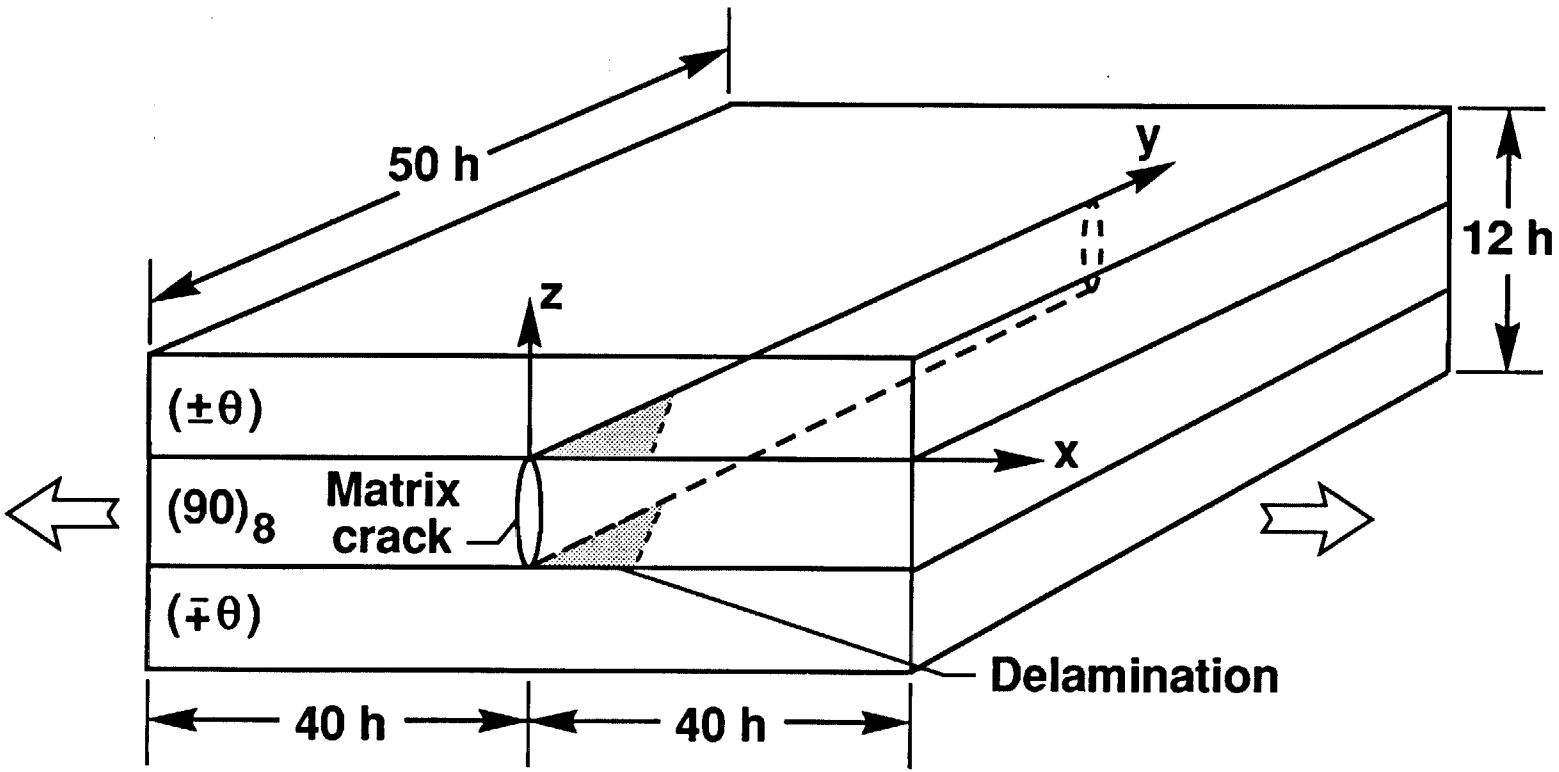

Fig. 4- Schematic of an inclined delamination, growing from a 90^{o} matrix crack.

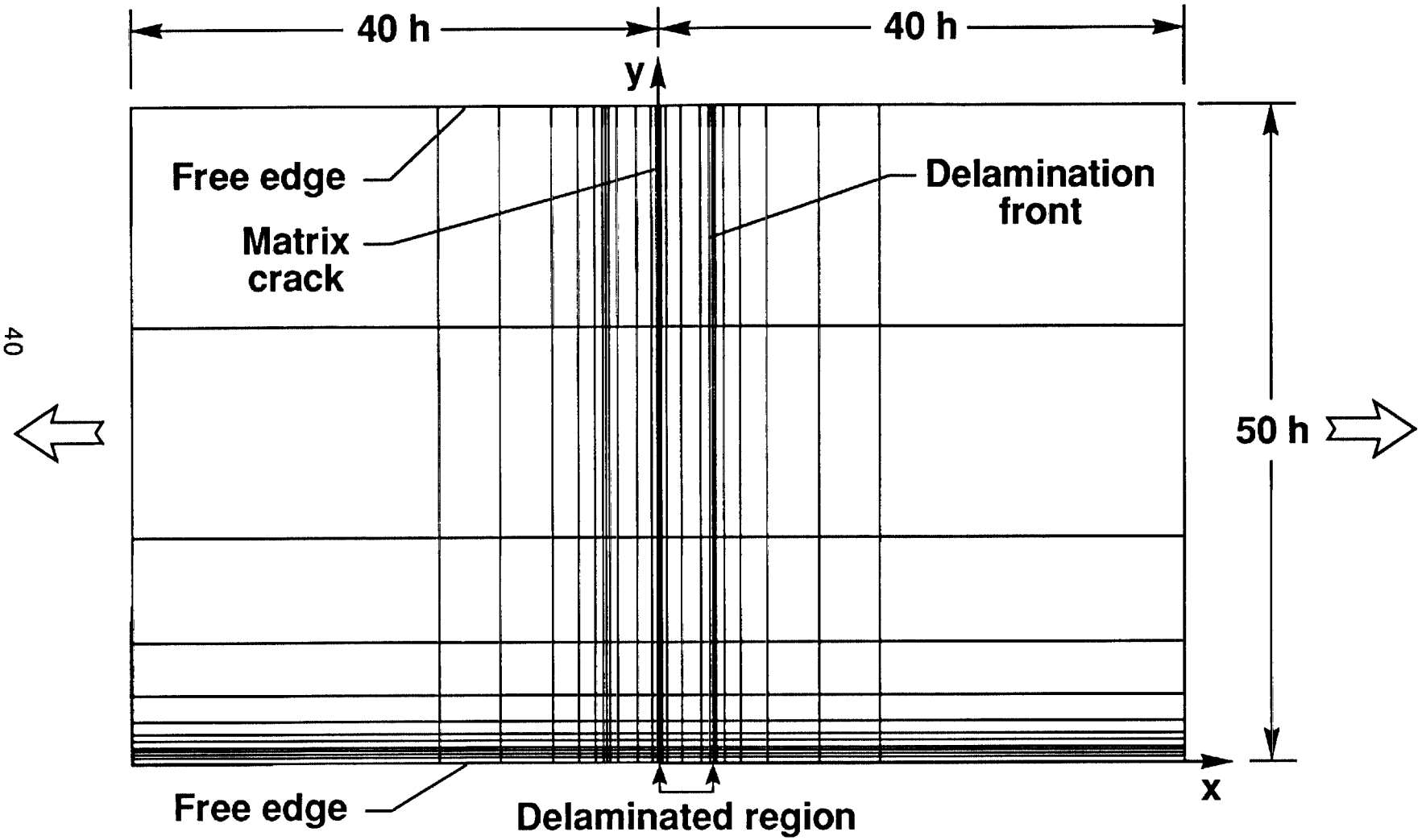

Fig. 5- Finite element mesh at delamination plane for a through-width uniform delamination.

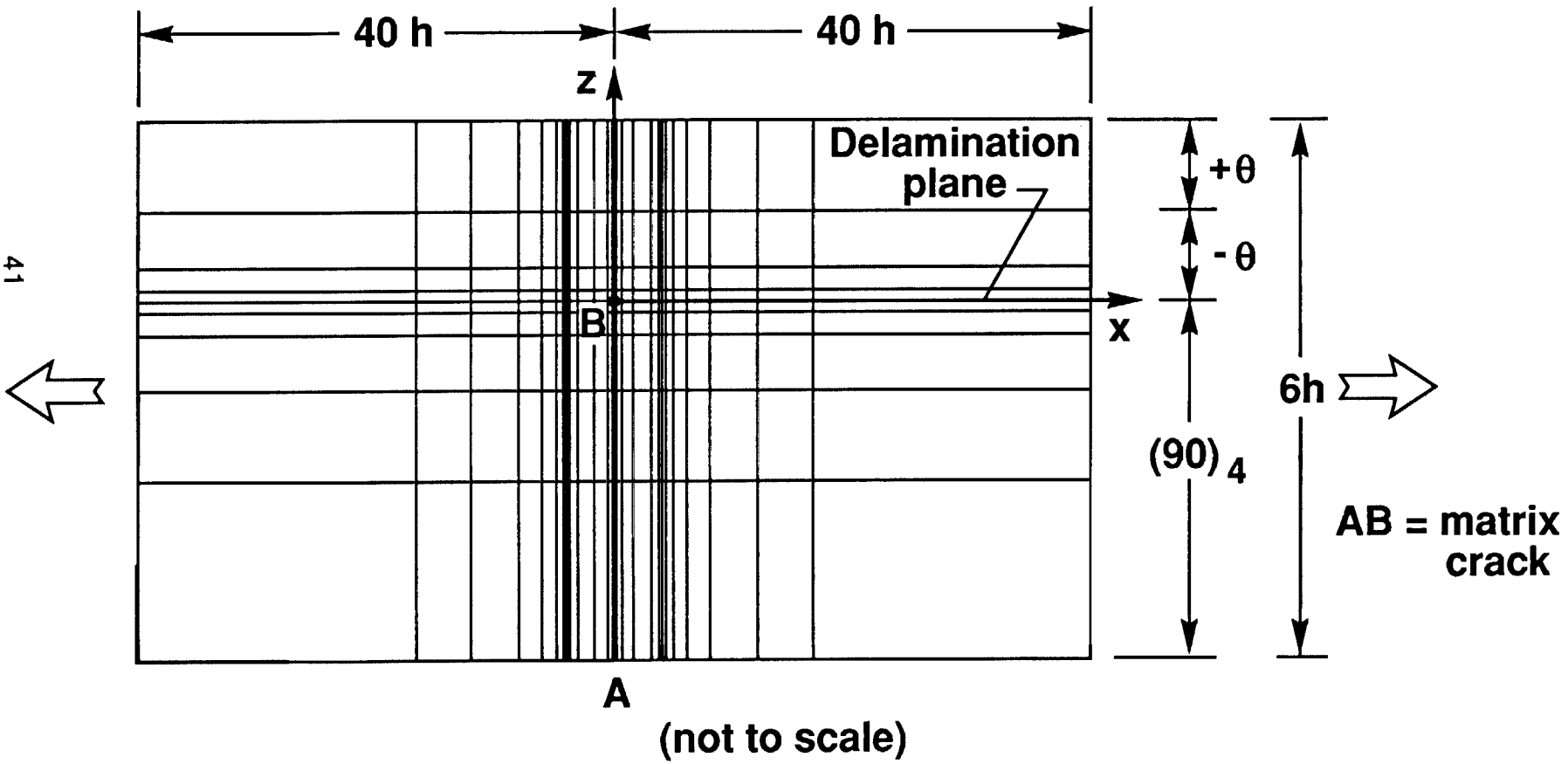

Fig. 6- Finite element discretization across laminate thickness.

: Not to scale :

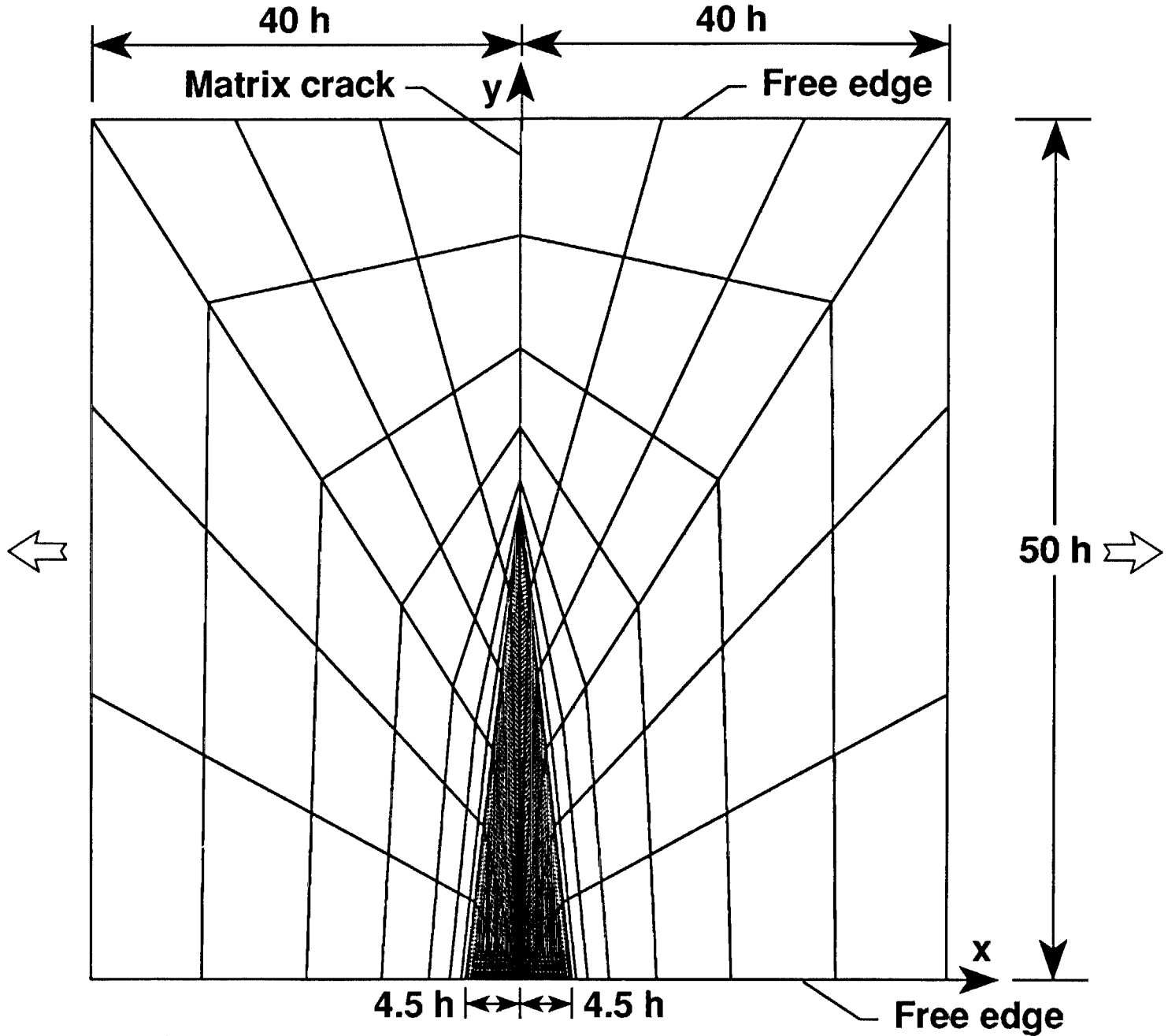

Fig. 7- Finite element mesh at delamination plane, for a delamination angle α=10.6°.

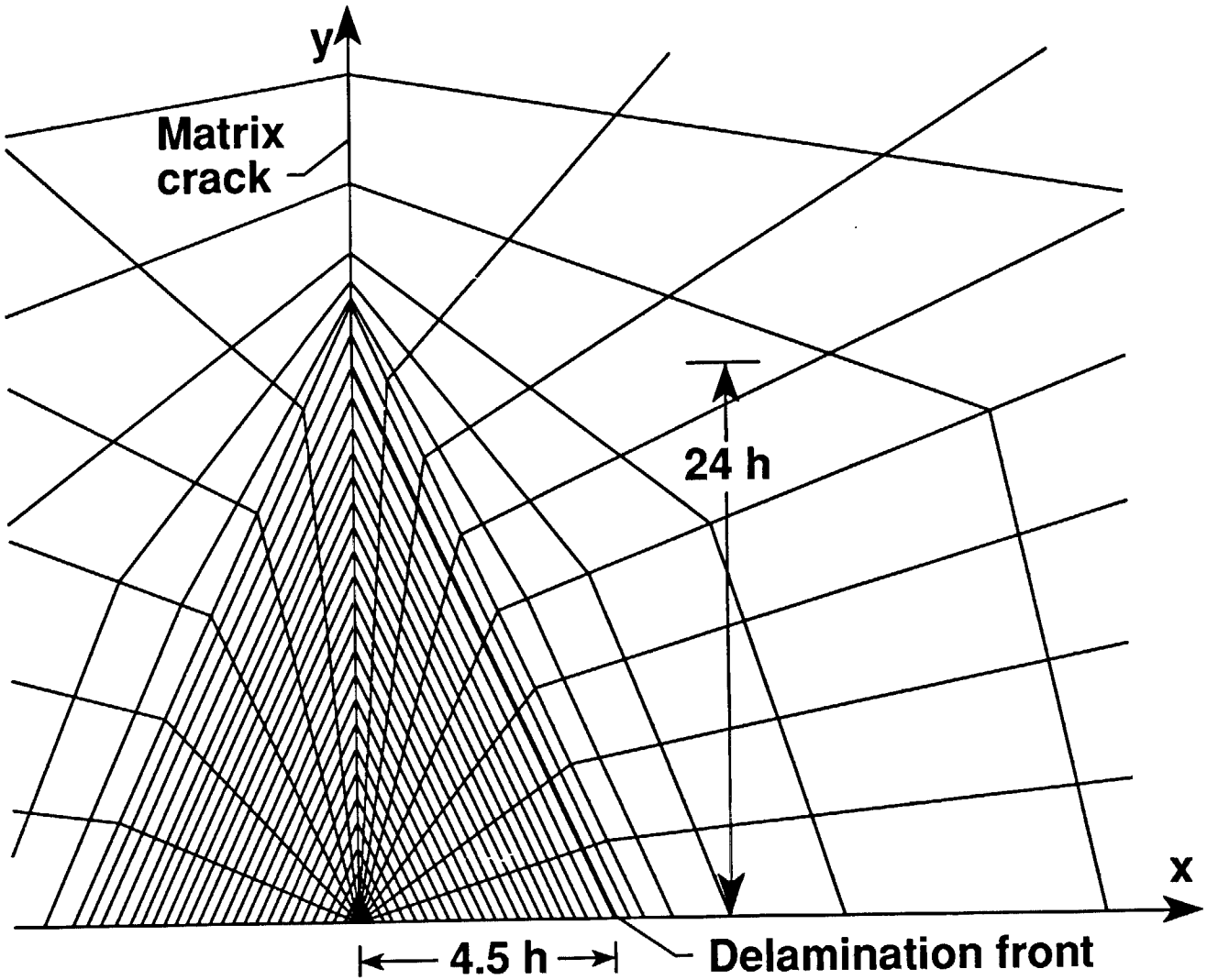

Fig. 8- Finite element mesh in the vicinity of delamination front, for a delamination angle α=10.6°.

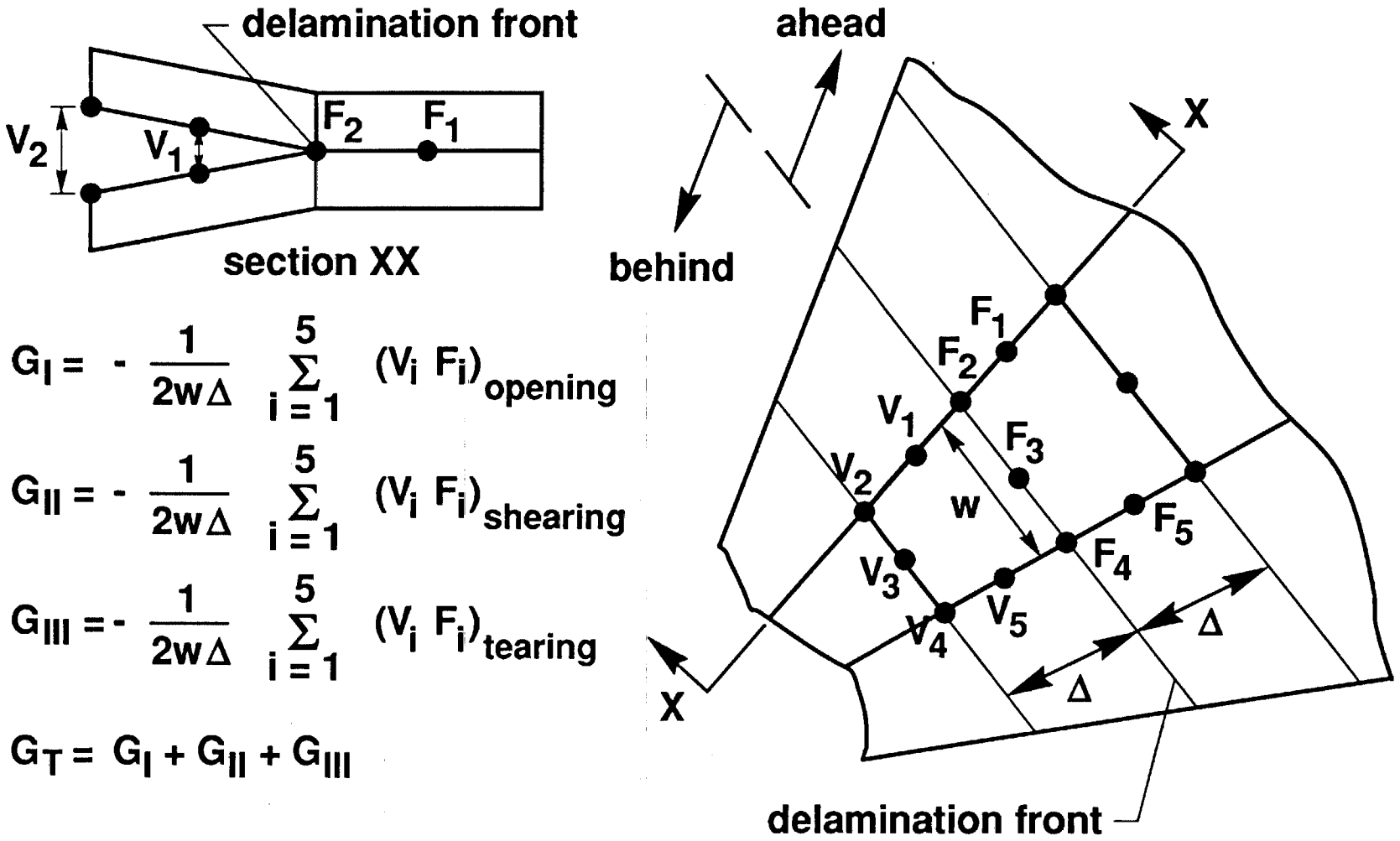

$$G_I = -\frac{1}{2w\Delta}\sum_{i=1}^{5}(V_i F_i)_{opening}$$

$$G_{II} = -\frac{1}{2w\Delta}\sum_{i=1}^{5}(V_i F_i)_{shearing}$$

$$G_{III} = -\frac{1}{2w\Delta}\sum_{i=1}^{5}(V_i F_i)_{tearing}$$

$$G_T = G_I + G_{II} + G_{III}$$

Fig. 9- Calculation of G using virtual crack closure technique.

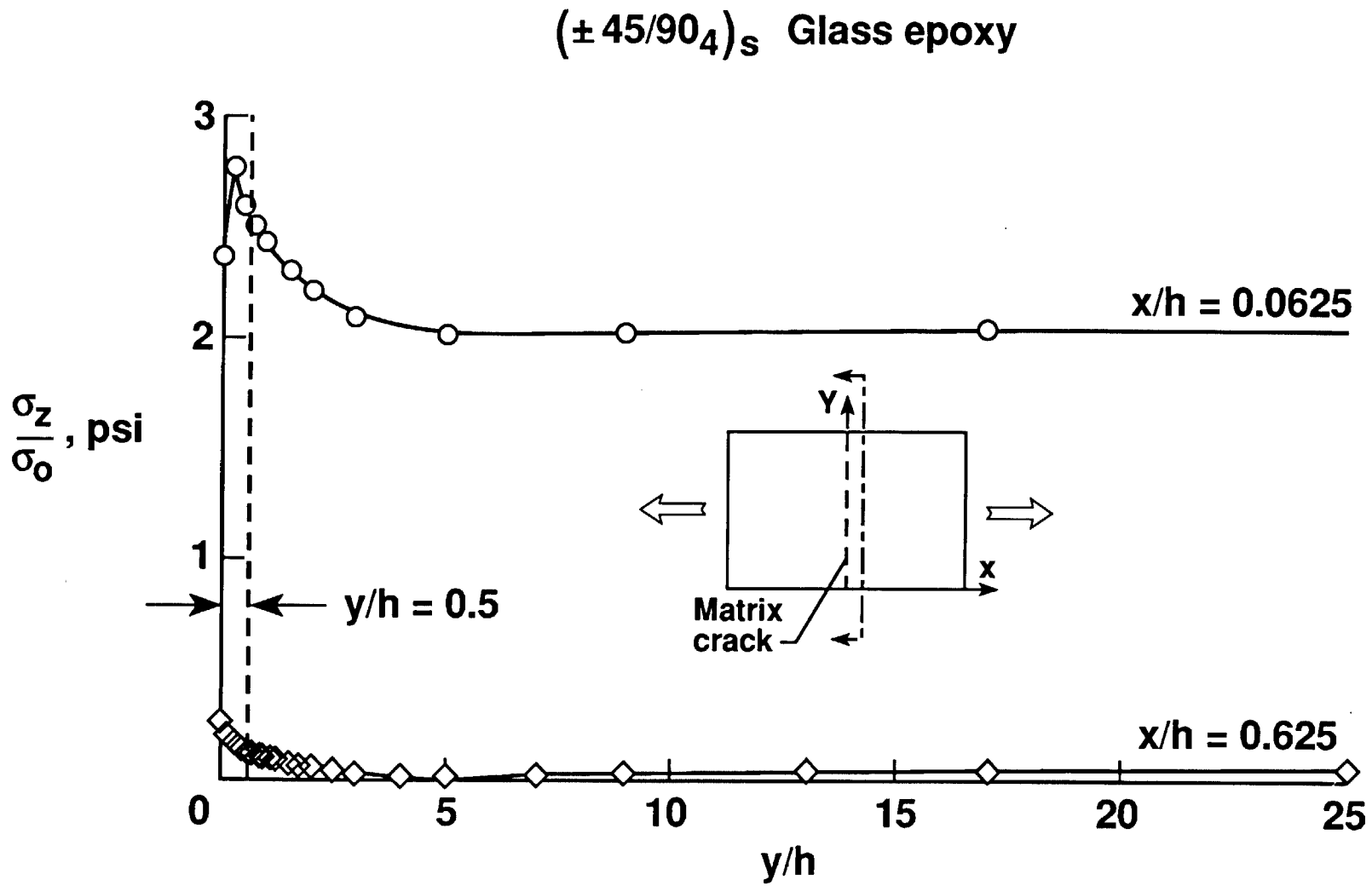

Fig. 10- Variation of normalized interlaminar normal stress in the -45/90 interface along laminate width.

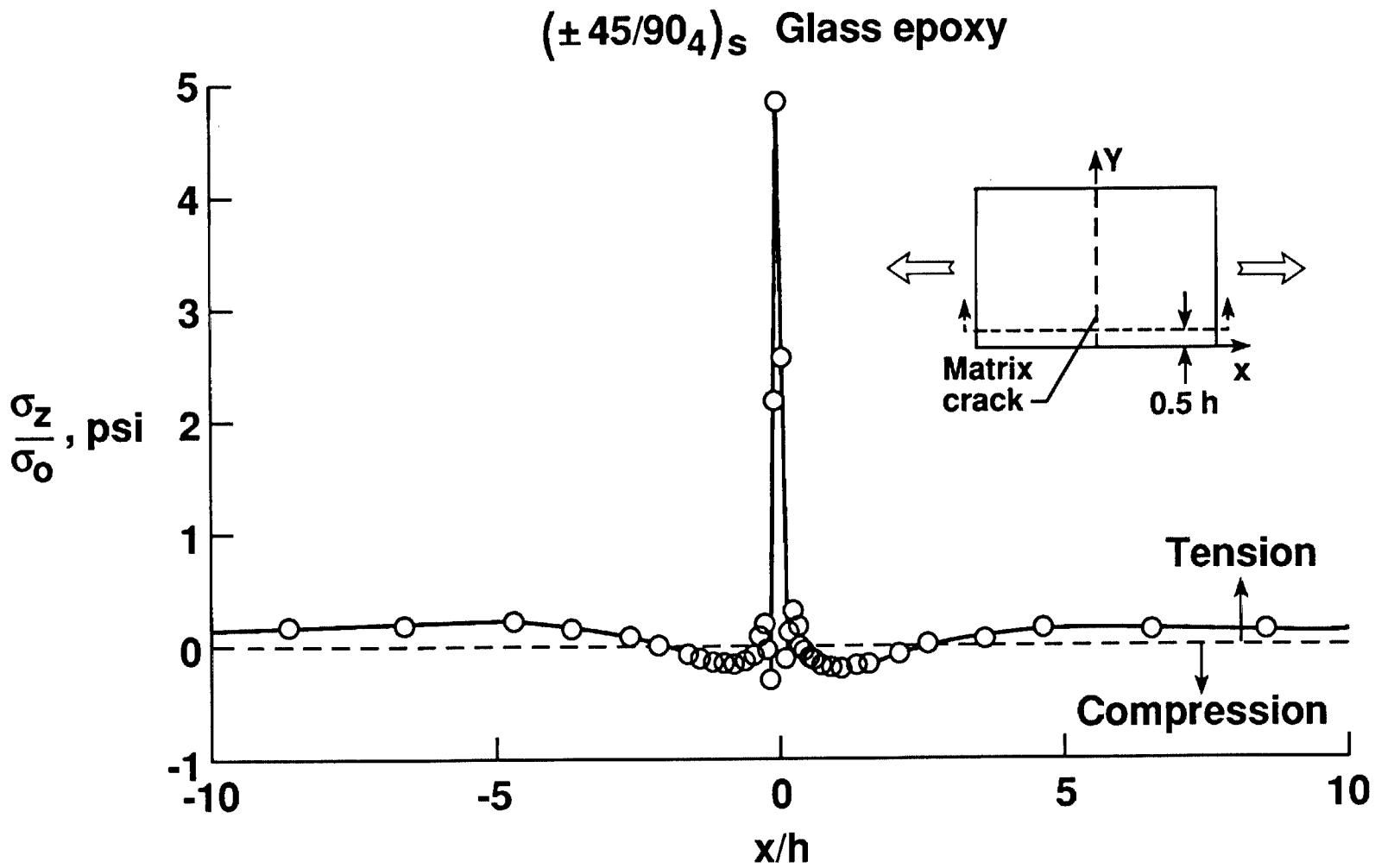

Fig. 11- Variation of normalized interlaminar normal stress in the -45/90 interface along laminate length.

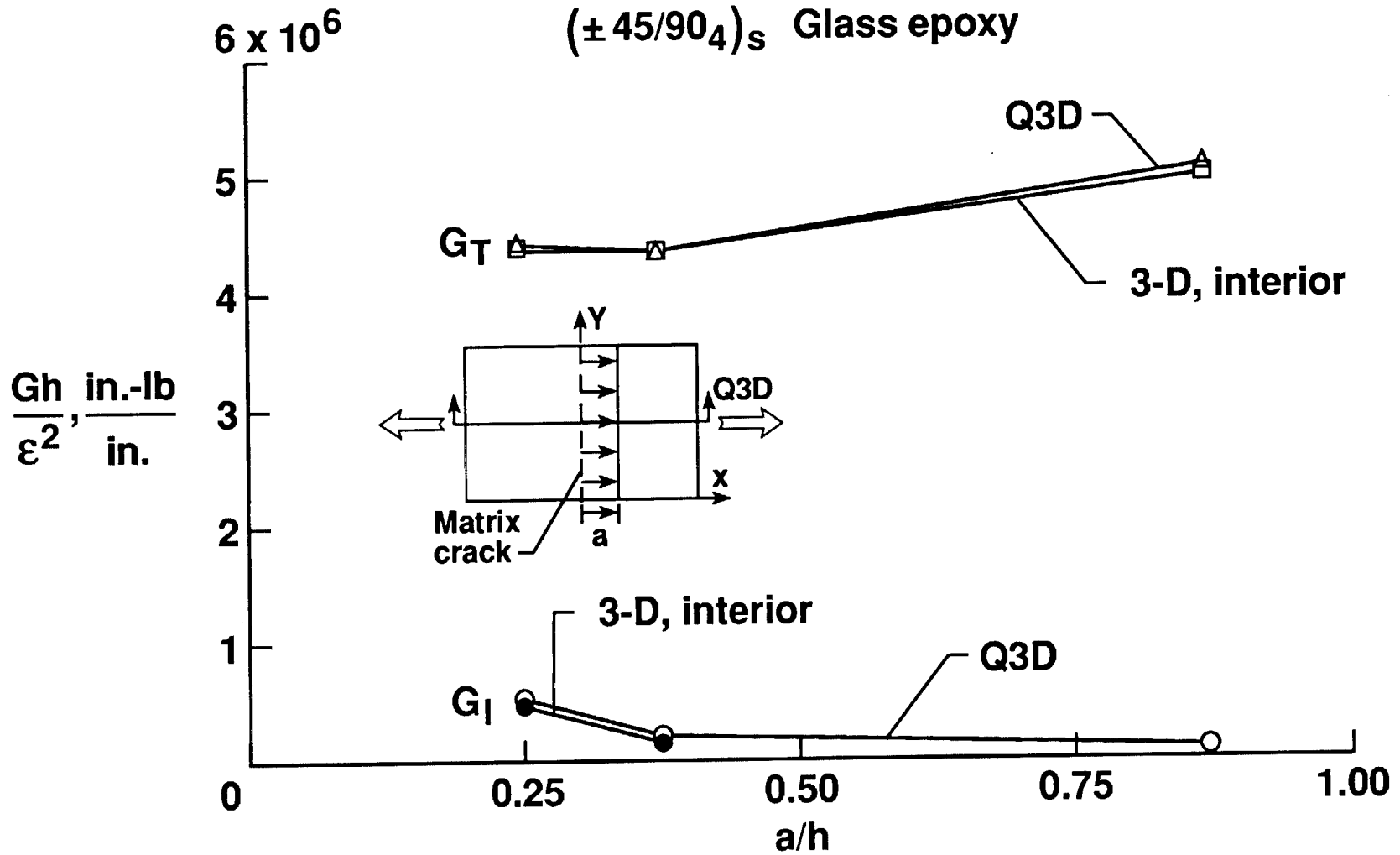

Fig. 12- Comparison of normalized G_I and G_T in laminate interior, using Q3D and 3-D finite element analyses.

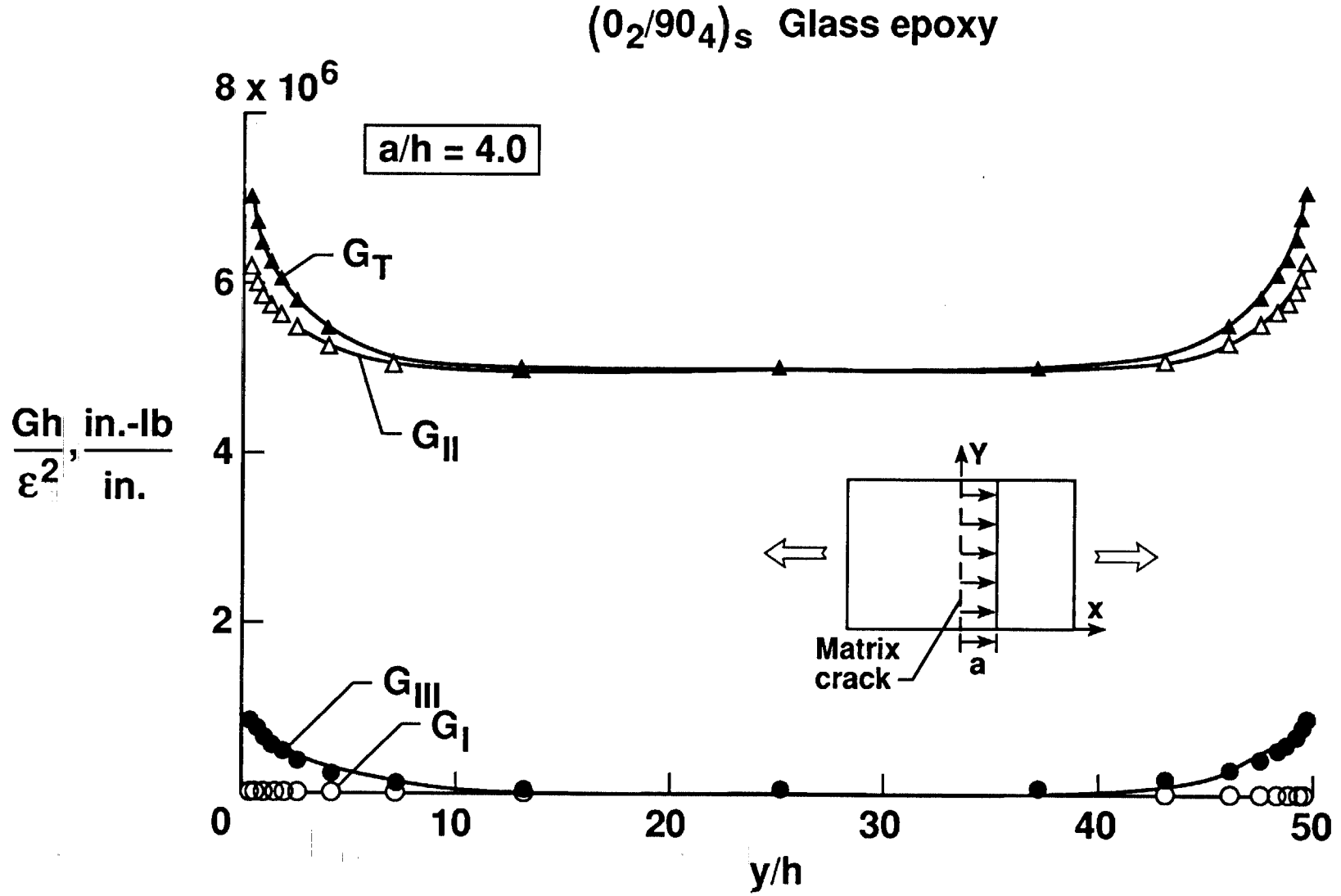

Fig. 13- Variation of normalized G along a uniform delamination front in Layup A, at a/h=4.0.

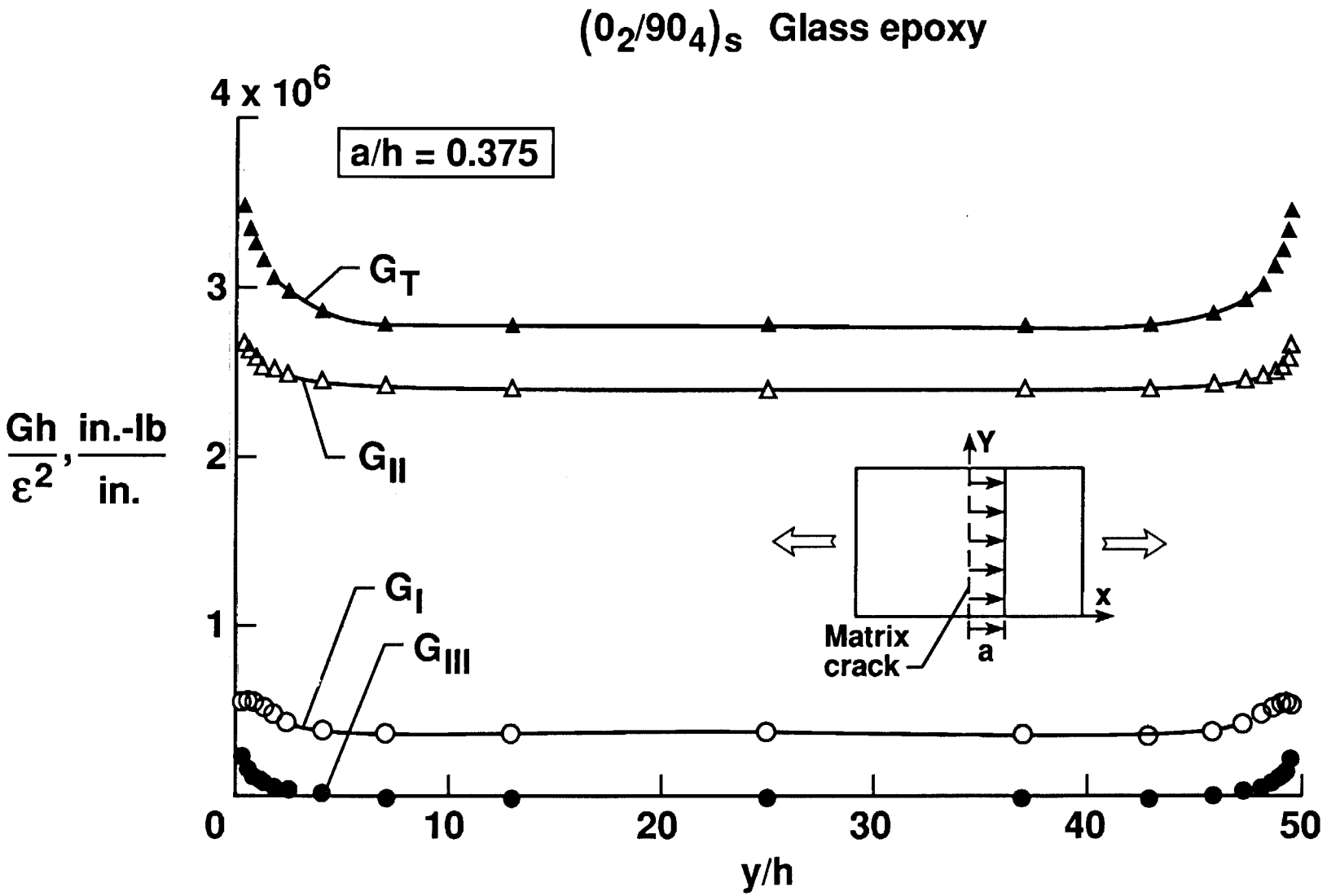

Fig. 14- Variation of normalized G along a uniform delamination front in Layup A, at a/h=0.375.

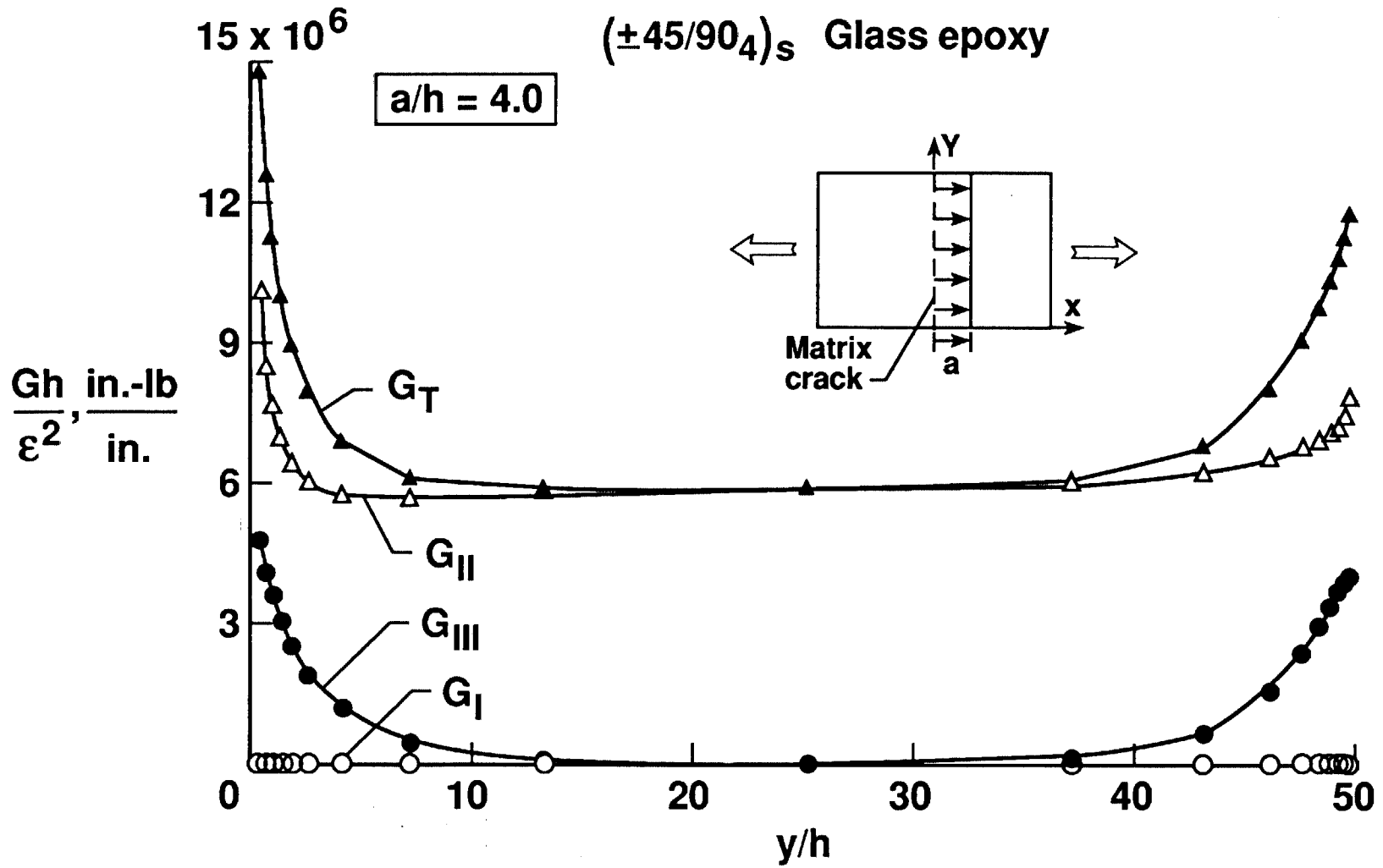

Fig. 15- Variation of normalized G along a uniform delamination front in Layup B, at a/h=4.0.

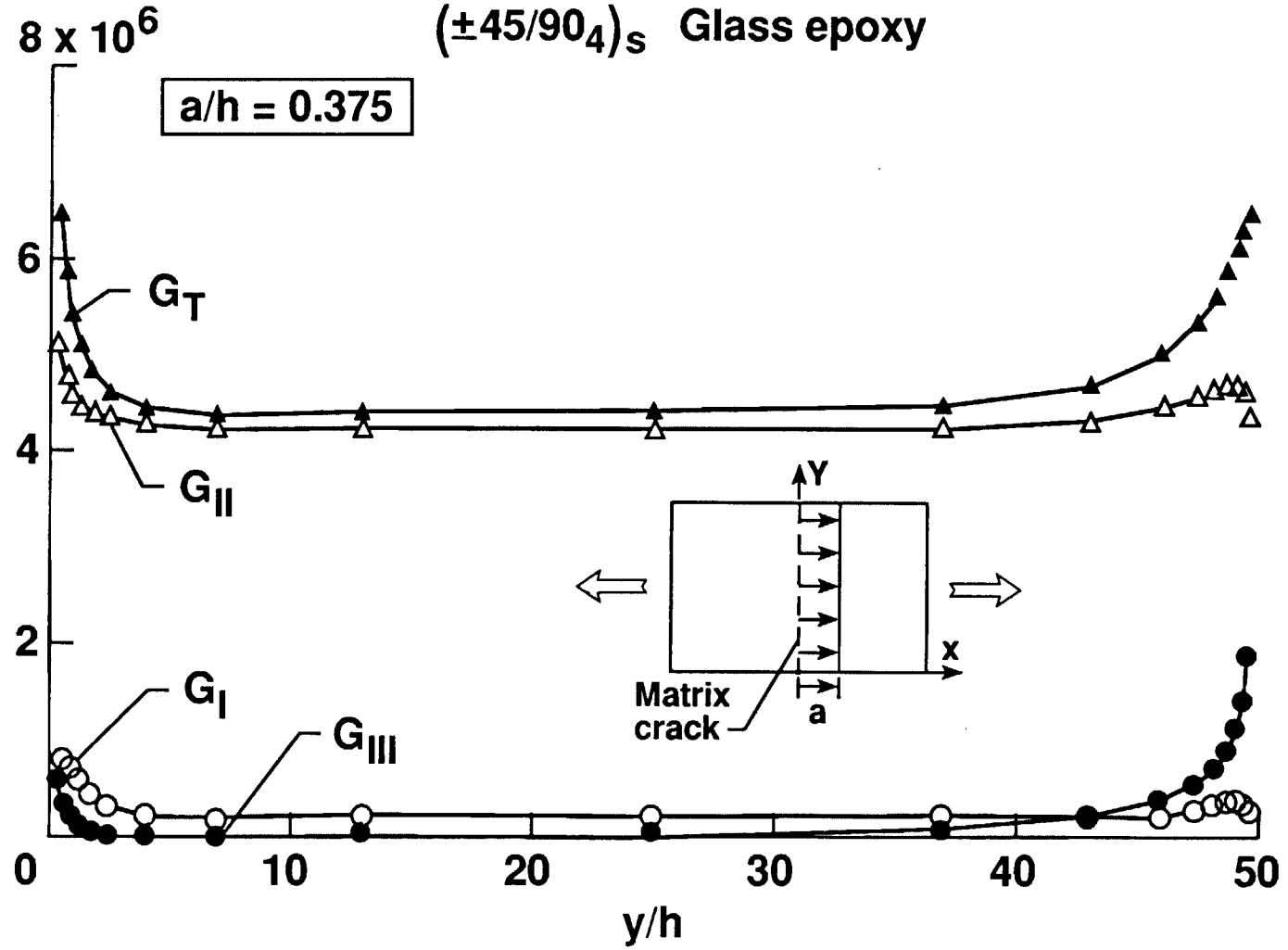

Fig. 16- Variation of normalized G along a uniform delamination front in Layup B, at a/h=0.375.

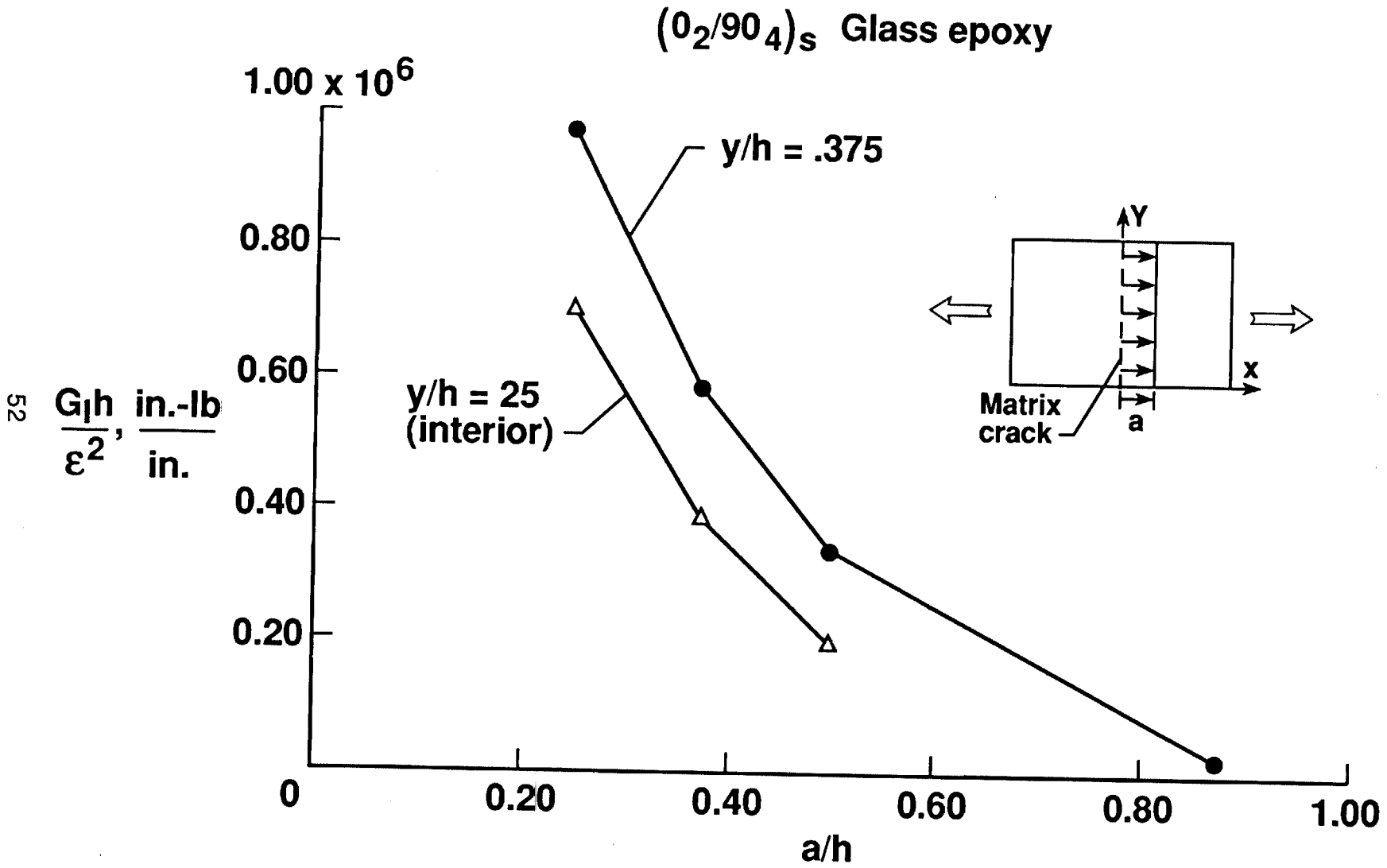

Fig. 17- Change in normalized G_I due to uniform delamination growth in Layup A.

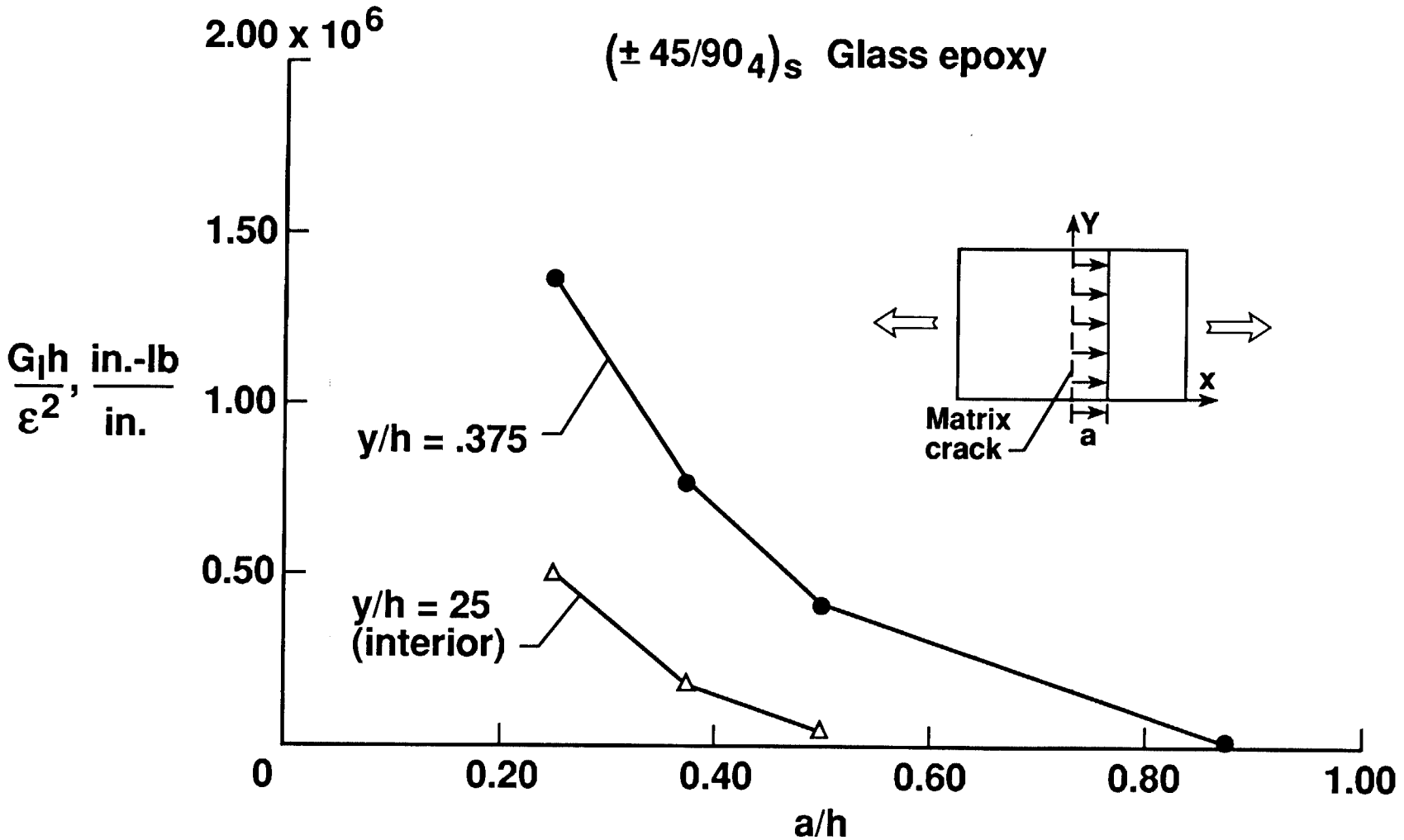

Fig. 18- Change in normalized G_I due to uniform delamination growth in Layup B.

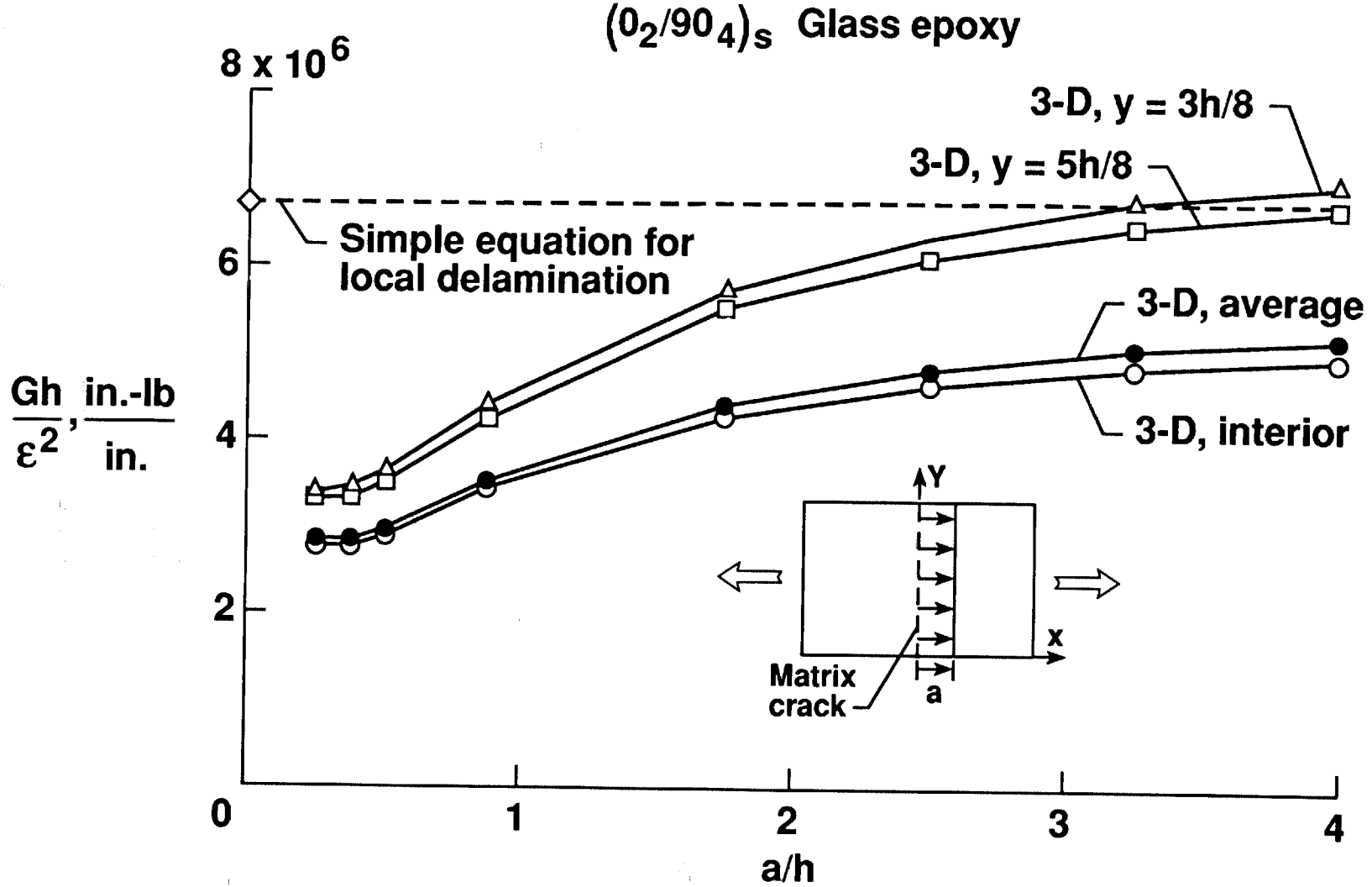

Fig. 19- Change in normalized G due to uniform delamination growth in Layup A.

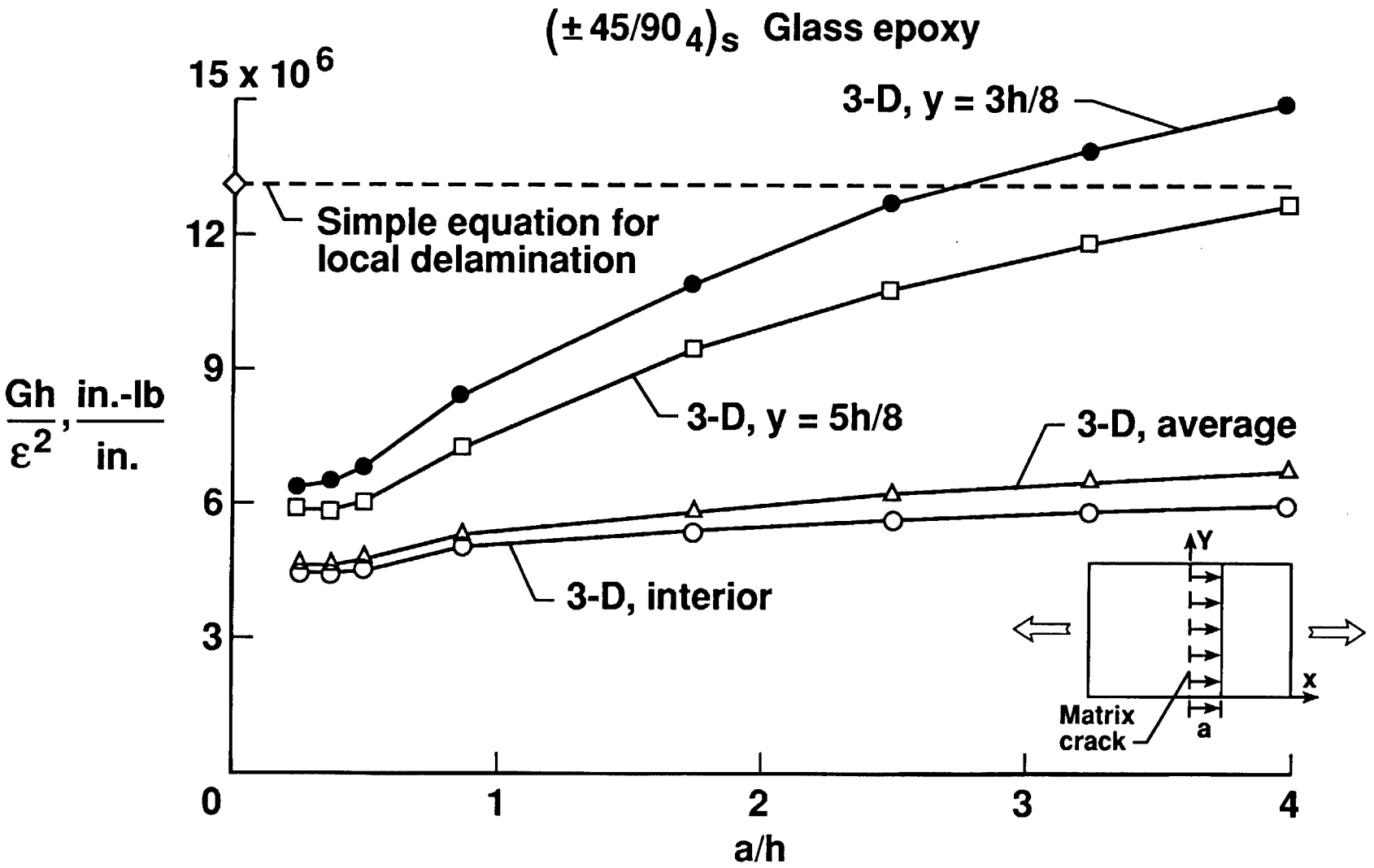

Fig. 20- Change in normalized G due to uniform delamination growth in Layup B.

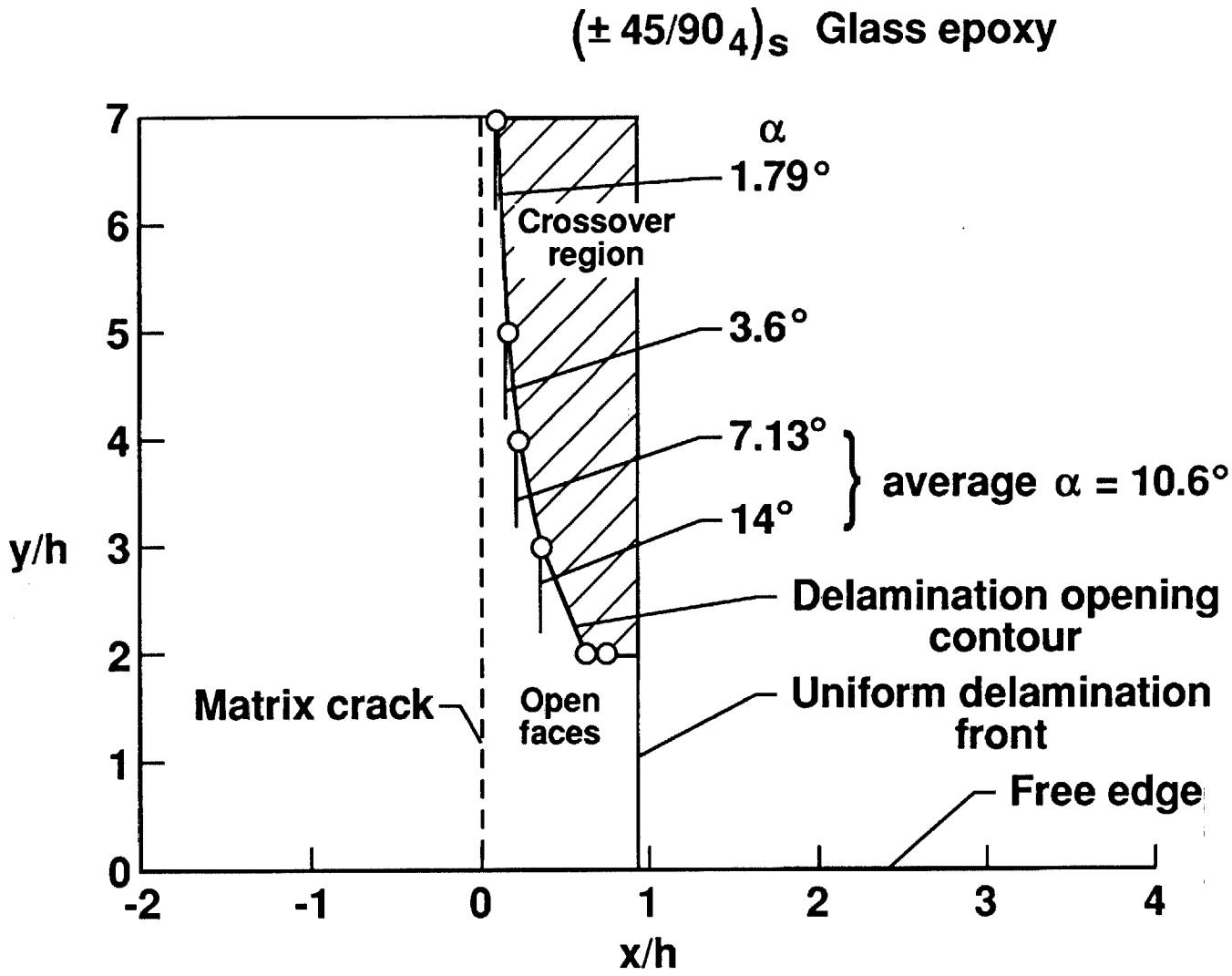

Fig. 21- Delamination contour near free edge, due to opening mode.

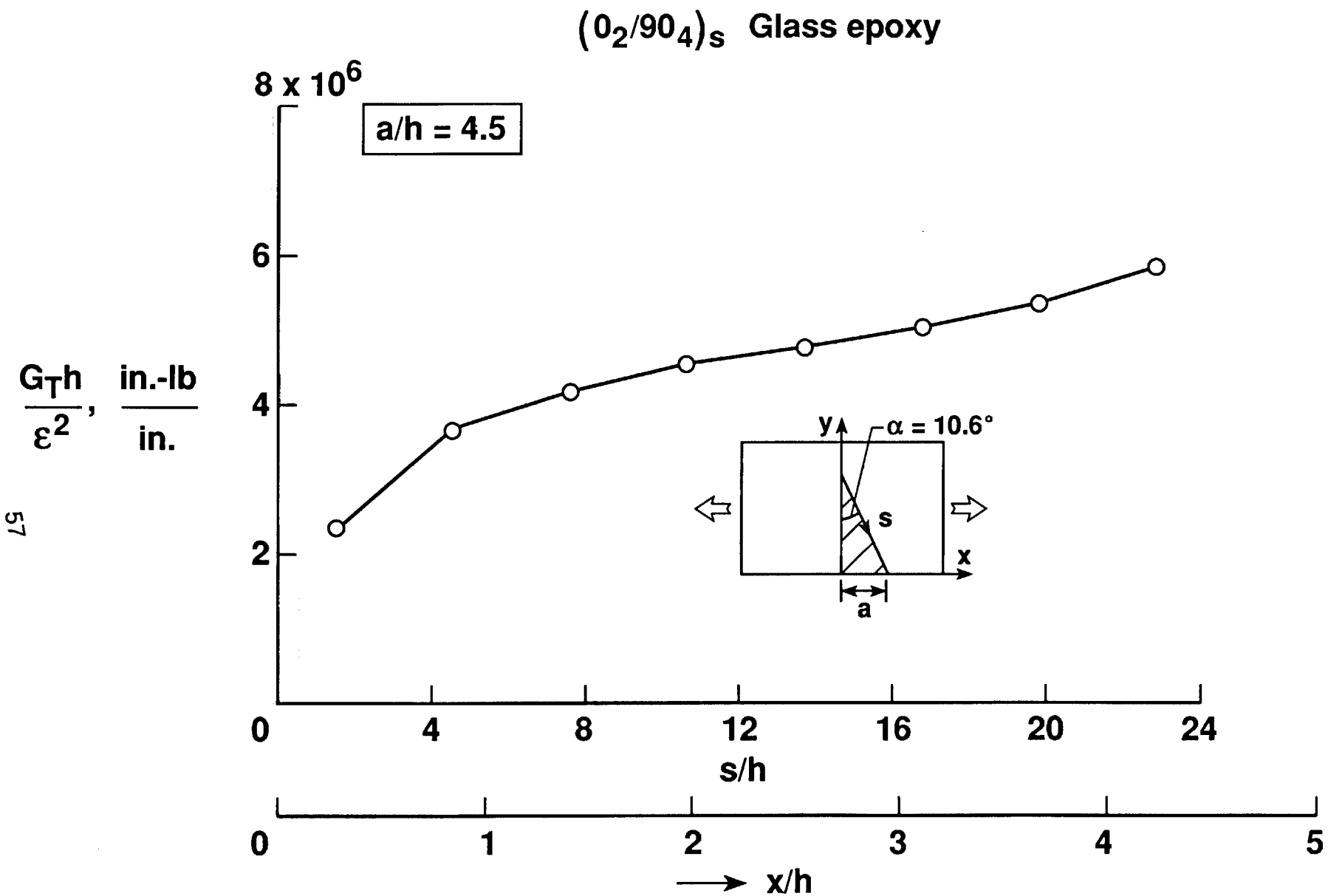

Fig. 22- Variation of normalized G_T along inclined delamination front for Layup A, (α=10.6°, and a/h=4.5).

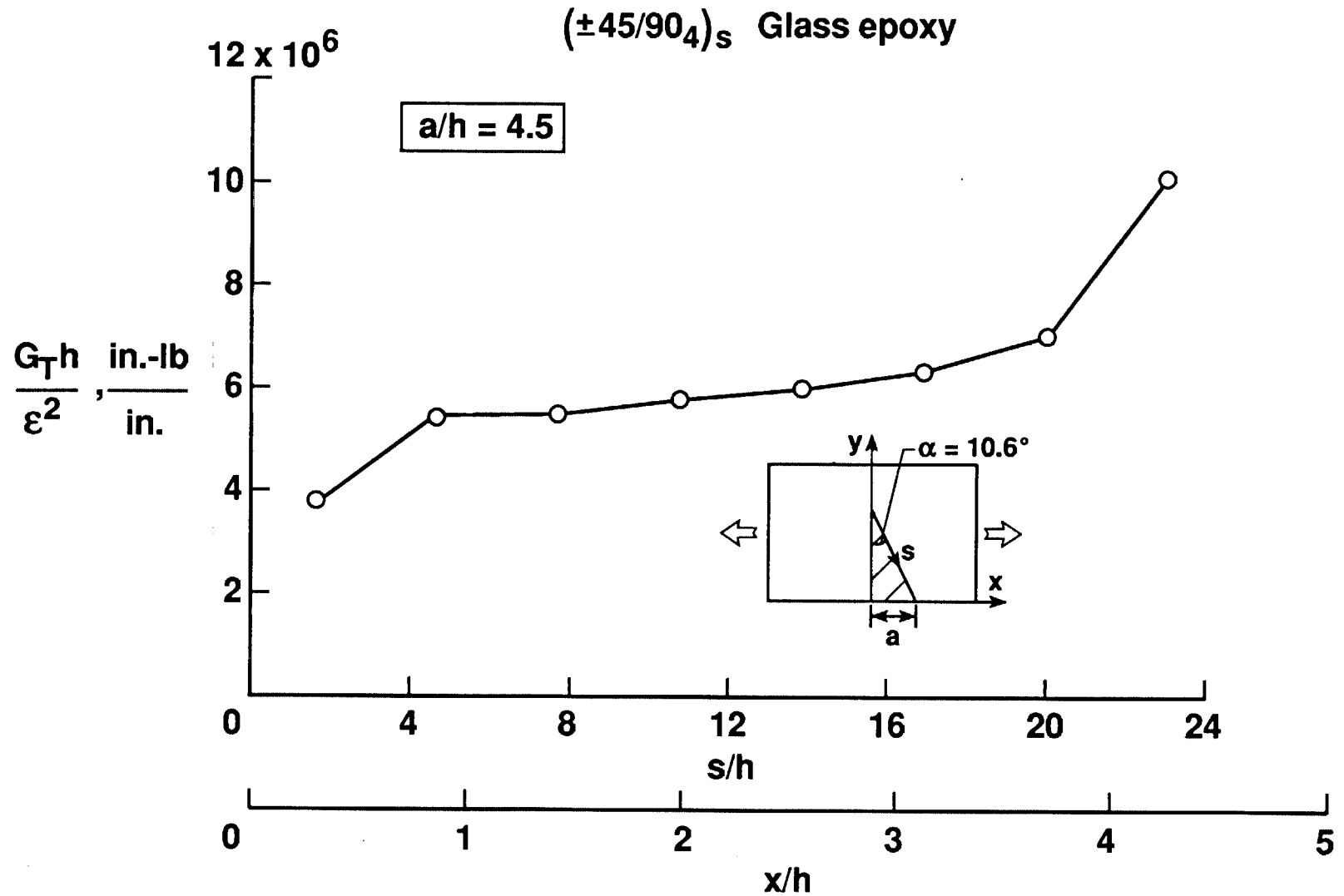

Fig. 23- Variation of normalized G_T along inclined delamination front for Layup B, (α=10.6°, and a/h=4.5).

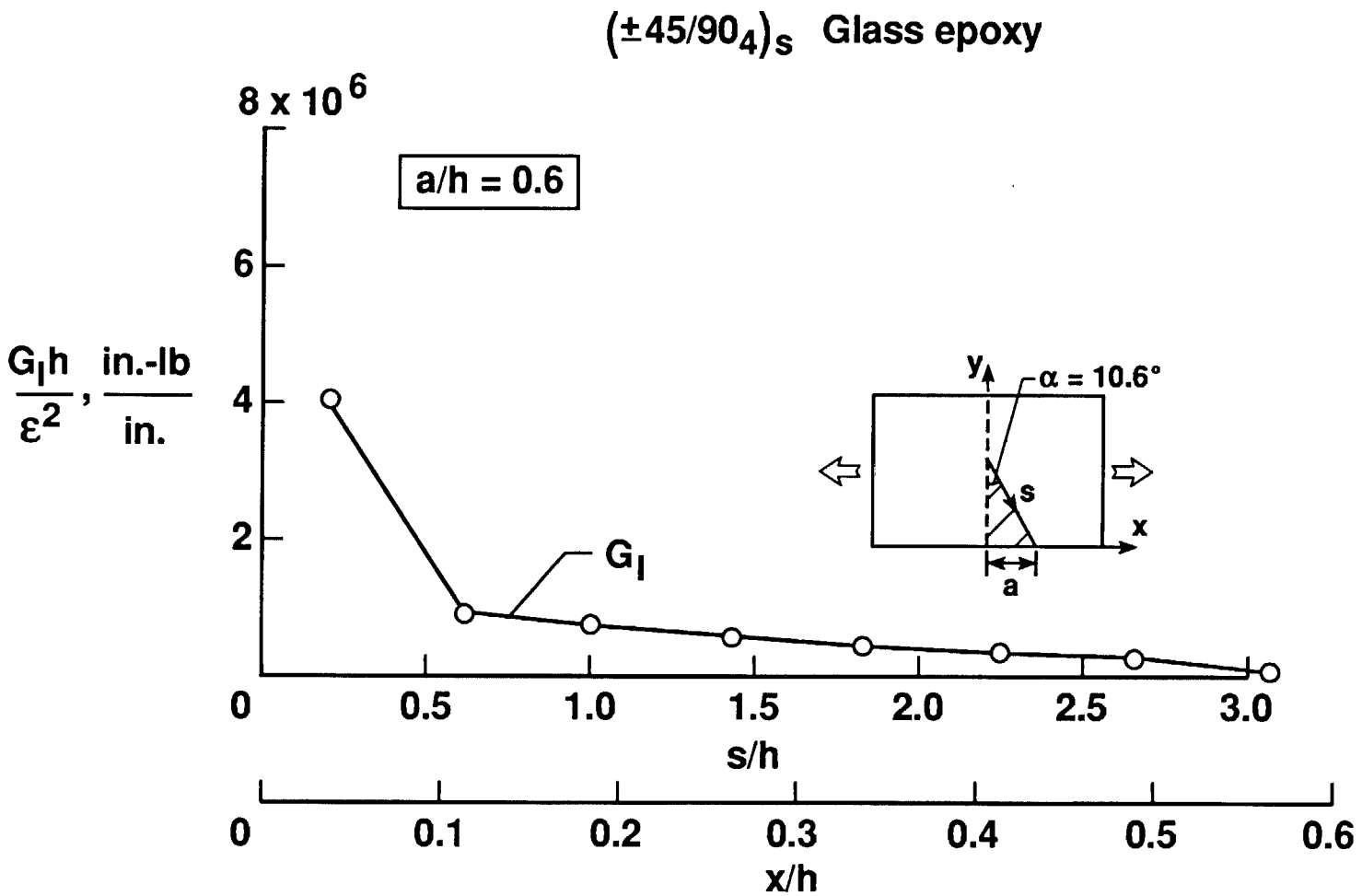

Fig. 24- Variation of normalized G_I along inclined delamination front for Layup B, (α=10.6°, and a/h=0.6).

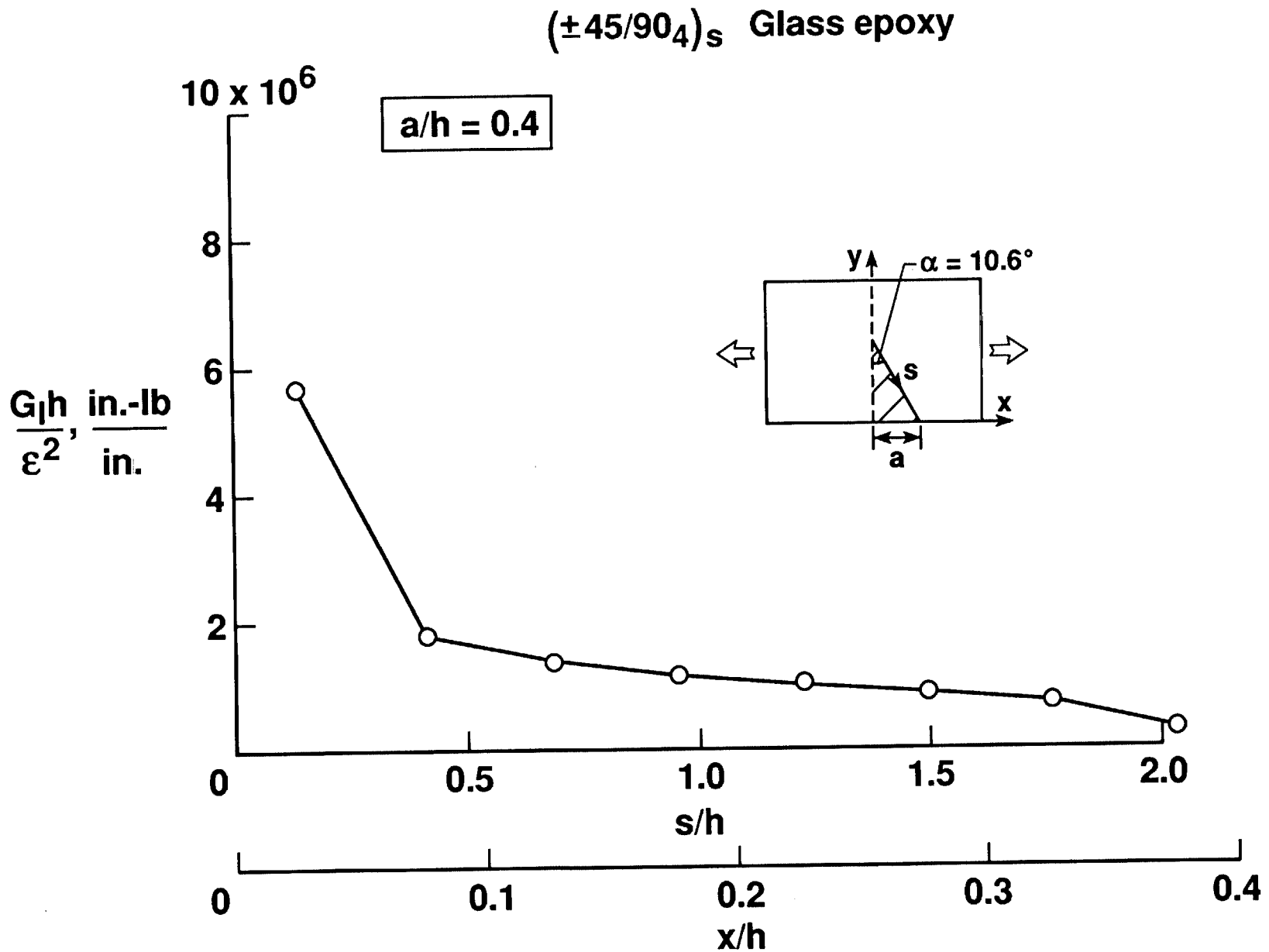

Fig. 25- Variation of normalized G_I along inclined delamination front for Layup B, (α=10.6°, and a/h=0.4).

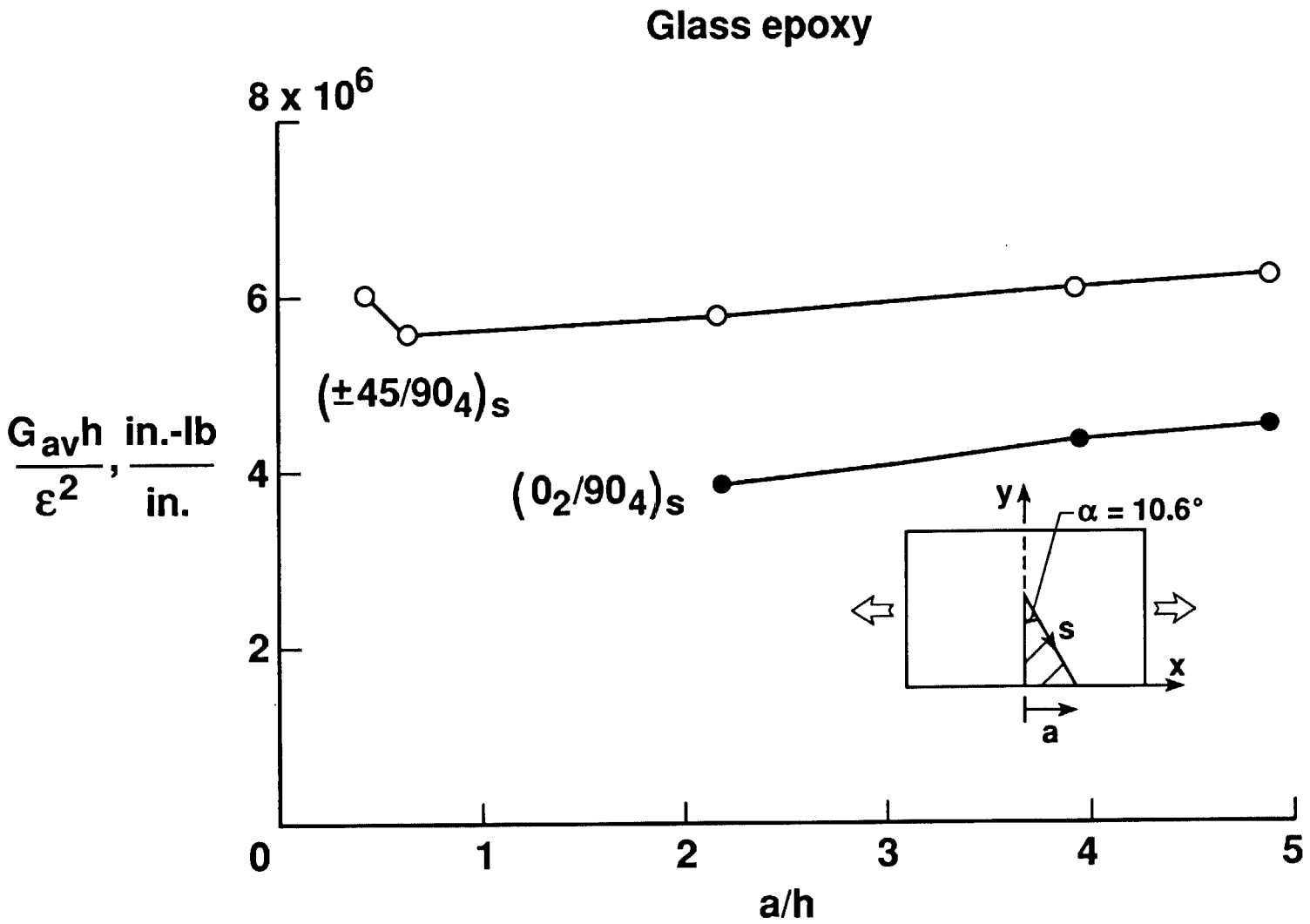

Fig. 26- Change in normalized G_{av} due to delamination growth at $\alpha=10.6^{o}$.

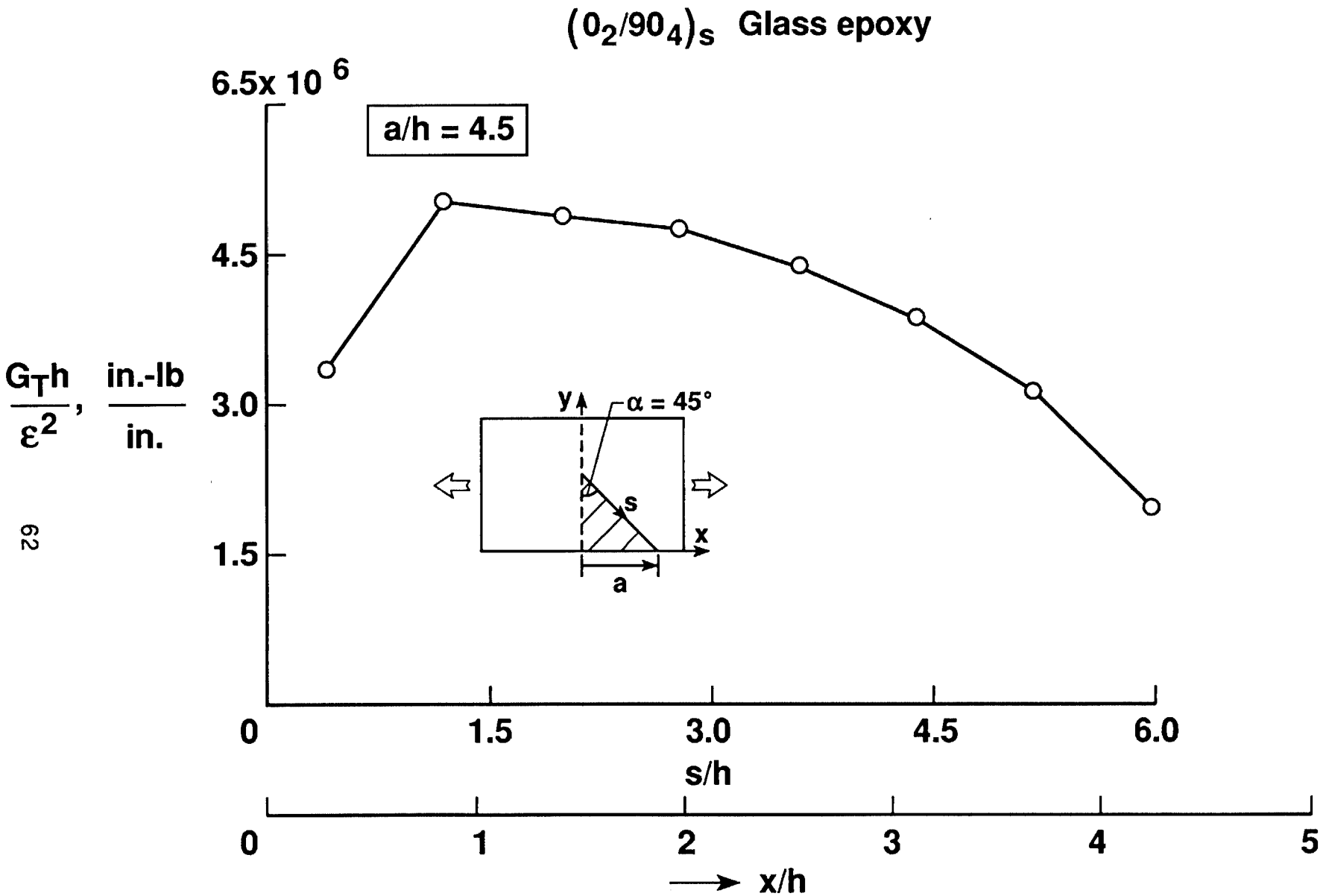

Fig. 27- Variation of normalized G_T along inclined delamination front for Layup A, (α=45°, and a/h=4.5).

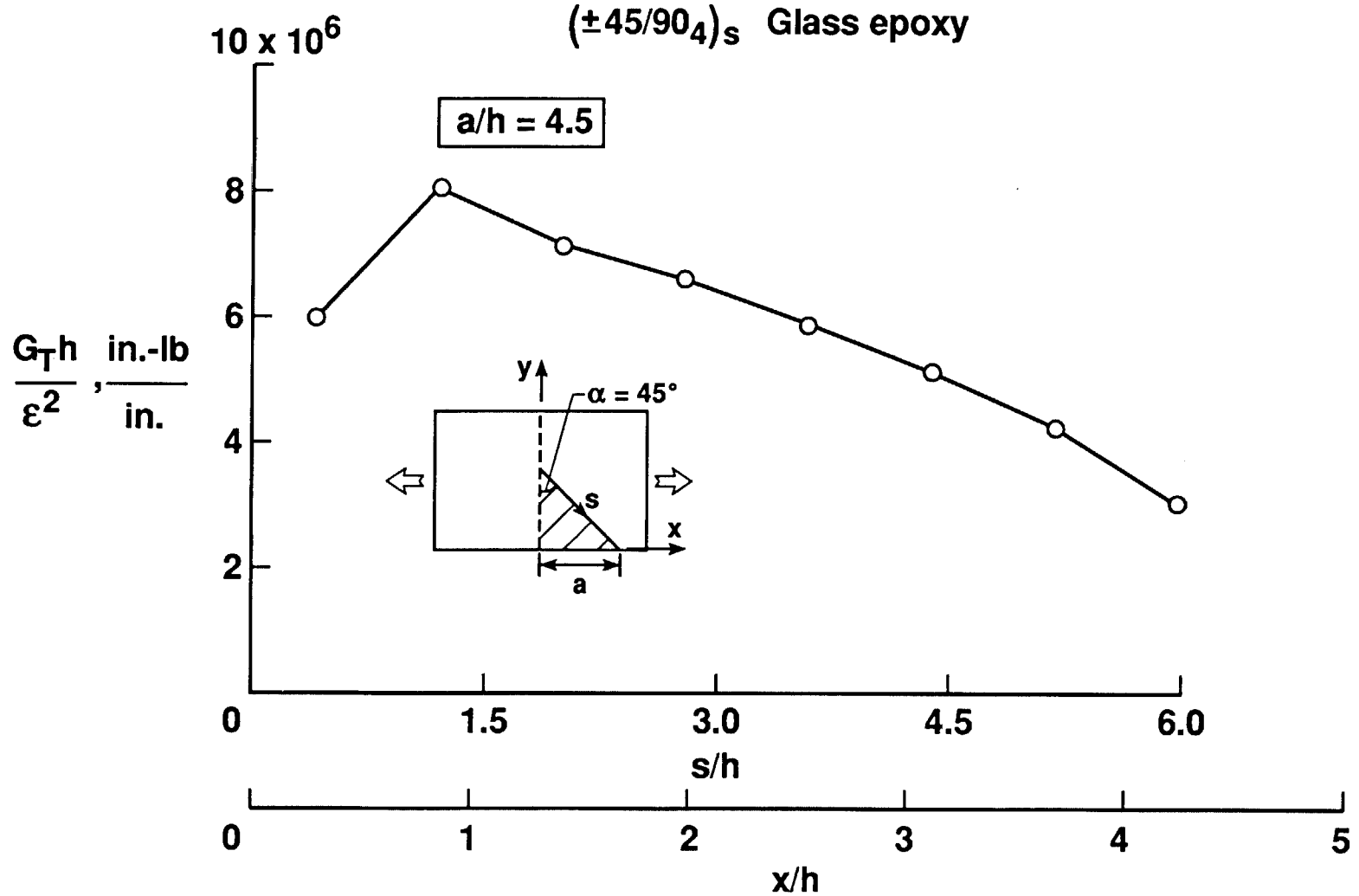

Fig. 28- Variation of normalized G_T along inclined delamination front for Layup B, (α=45°, and a/h=4.5).

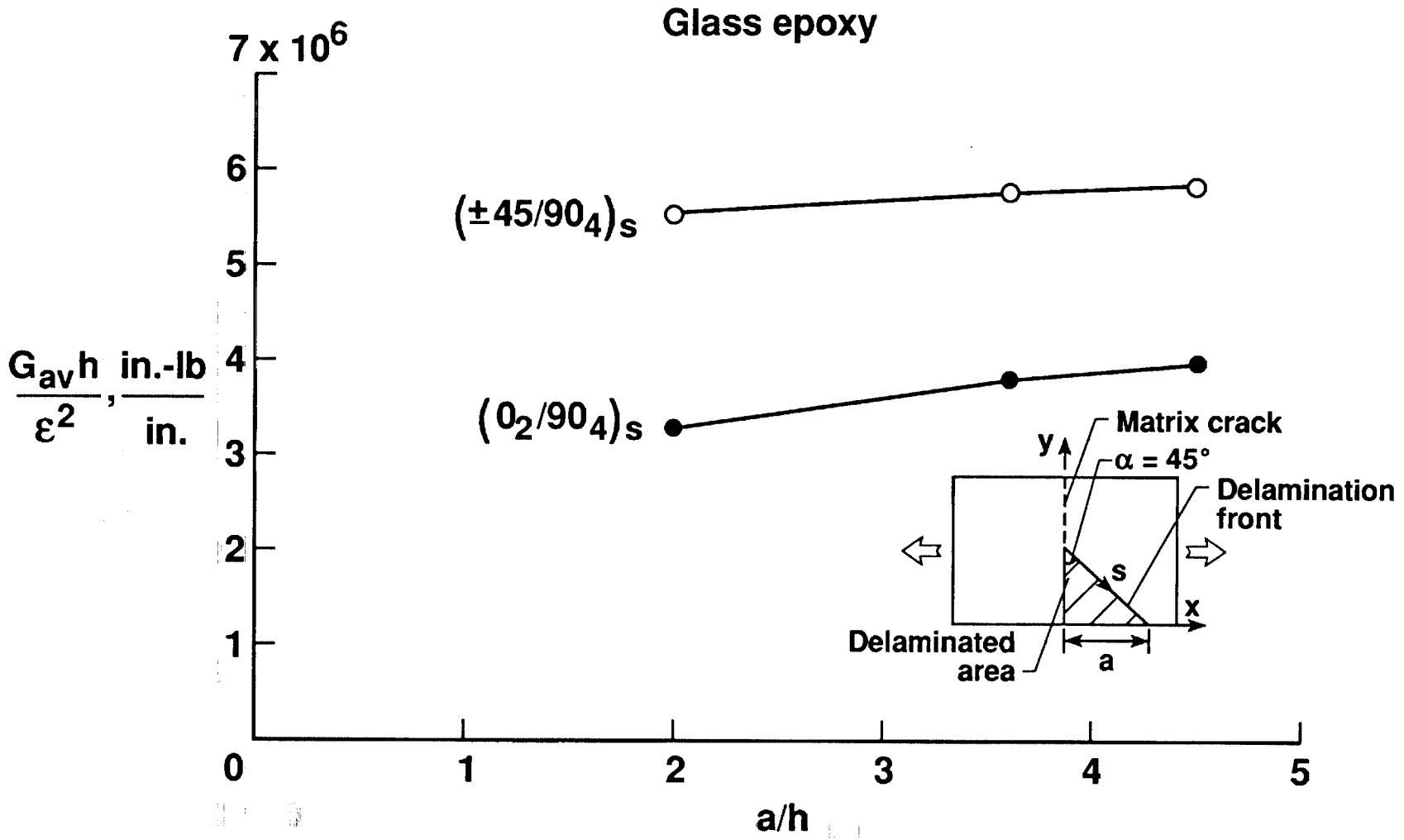

Fig. 29- Change in normalized G_{av} due to delamination growth at $\alpha=45^{o}$.

NASA National Aeronautics and Space Administration

Report Documentation Page

1. Report No.	2. Government Accession No.	3. Recipient's Catalog No.
NASA TM-102591 AVSCOM TM-90-B-002		

4. Title and Subtitle

Combined Effect of Matrix Cracking and Stress-Free Edge on Delamination

5. Report Date

March 1990

6. Performing Organization Code

7. Author(s)

S. A. Salpekar* and T. K. O'Brien**

8. Performing Organization Report No.

10. Work Unit No.

505-63-01-05

9. Performing Organization Name and Address

NASA Langley Research Center, Hampton, VA 23665-5225
U.S. Army Aviation Research Technology Activity (AVSCOM)
Aerostructures Direcorate
Hampton, VA 23665-5225

11. Contract or Grant No.

13. Type of Report and Period Covered

Technical Memorandum

12. Sponsoring Agency Name and Address

National Aeronautics and Space Administration
Washington, DC 20546
U.S. Army Aviation Systems Command
St. Louis, MO 63166

14. Sponsoring Agency Code

15. Supplementary Notes

*S.A. Salpekar, Analytical Services and Materials, Inc., Hampton, VA 23666
**T. K. O'Brien, U.S. Army Aerostructures Directorate, USAARTA-AVSCOM, Langley Research Center, Hampton, VA 23665

16. Abstract

The effect of the stress-free edge on the growth of local delaminations initiating from a matrix crack in $(0_2/90_4)_S$ and $(\pm 45.90_4)_S$ glass epoxy laminates is investigated using 3D finite-element analysis. The presence of high interlaminar normal stresses at the intersection (corner) of the matrix crack with the stress-free edge, suggests that a mode I delamination may initiate at the corners. The strain energy release rates (G) were calculated by modeling a uniform through-width delamination and two inclined delaminations at 10.6° and 45° to the matrix crack. All components of G have high values near the free edges. The mode I component of G is high at small delamination length and becomes zero for a delamination length of one-ply thickness. The total G values near the free edge agreed well with previously derived closed form solution. The quasi-3D solutions agreed well with the 3-D interior solutions.

17. Key Words (Suggested by Author(s))

Stress-free edge
Matrix crack
Delamination
Strain energy release rate
Three-dimensional analysis

18. Distribution Statement

Unclassified - Unlimited
Subject Category - 24

19. Security Classif. (of this report)	20. Security Classif. (of this page)	21. No. of pages	22. Price
Unclassified	Unclassified	65	A04

NASA FORM 1626 OCT 86